Kinetic modeling of low-pressure nitrogen discharges and post-discharges

V. Guerra[1,a], P.A. Sá[2], and J. Loureiro[1]

[1] Centro de Física dos Plasmas, Instituto Superior Técnico, 1049-001 Lisboa, Portugal
[2] Dep. de Física, Faculdade de Engenharia, Universidade do Porto, 4200-465 Porto, Portugal

Abstract. The kinetic modeling of low-pressure ($p \sim 1-10$ torr) stationary nitrogen discharges and the corresponding afterglows is reviewed. It is shown that a good description of the overall behavior of nitrogen plasmas requires a deep understanding of the coupling between different kinetics. The central role is played by ground-state vibrationally excited molecules, $N_2(X\ ^1\Sigma_g^+, v)$, which have a strong influence on the shape of the electron energy distribution function, on the creation and destruction of electronically excited states, on the gas heating, dissociation and on afterglow emissions. $N_2(X\ ^1\Sigma_g^+, v)$ molecules are actually the hinge ensuring a strong link between the various kinetics. The noticeable task done by electronically excited metastable molecules, in particular $N_2(A\ ^3\Sigma_u^+)$ and $N_2(a'\ ^1\Sigma_u^-)$, is also pointed out. Besides contributing to the same phenomena as vibrationally excited molecules, these electronic metastable states play also a categorical role in ionization. Furthermore, vibrationally excited molecules in high v levels are in the origin of the peaks observed in the flowing afterglow for the concentrations of several species, such as $N_2(A\ ^3\Sigma_g^+)$, $N_2(B\ ^3\Pi_g)$, $N_2^+(B\ ^2\Sigma_u^+)$ and electrons, which occur downstream from the discharge after a dark zone as a consequence of the V-V up-pumping mechanism.

PACS. 52.20.-j Elementary processes in plasmas – 52.80.-s Electric discharges – 82.33.Xj Plasma reactions (including flowing afterglow and electric discharges)

1 Introduction

Nitrogen discharges and their afterglows have been the subject of a huge number of studies already for many decades. Even though, they have not lost interest and keep attracting scientists and researchers nowadays. For example, it is extremely likely to find articles about nitrogen in any reference international journal devoted to gas discharges or plasma science published in 2004. Why is that so? On one hand, because nitrogen is very important in different applications. On the other hand, because nitrogen plasmas form a very rich and complex medium for fundamental research. So rich that some very basic but critical processes, such as dissociation and ionization, are not yet completely understood.

The complexity of nitrogen arises from the strong coupling existing between different kinetics, such as electron, vibrational, chemical and surface kinetics. To get an overall picture of nitrogen discharges and afterglows it is thus necessary to understand the core of each of these kinetics, as well as the way each of them interacts with the others. At least since the 80s many groups have investigated in depth some of these kinetics, both theoretically and

experimentally. Unfortunately, with the advent of more sophisticated and global models, some fundamental issues seem to have been "forgotten" nowadays and it is common to find misinterpretations and misconceptions in recent works. Two examples of the most frequent are the invocation of vibrational dissociation in conditions where it cannot hold and equivocal explanations related to the role of associative ionization.

At present, it is possible to have a comprehensive view on the interplay of the different kinetics involved in nitrogen discharges and post-discharges, putting together results from several partial investigations. The first purpose of this review article is to describe and explain, in an unified way, the basic trends of the behavior of nitrogen plasmas, giving physical insight into the different phenomena. The emphasis must be given to the central role accomplished by vibrationally excited molecules of the electronic ground-state, $N_2(X\ ^1\Sigma_g^+, v)$, and the electronic metastable states $N_2(A\ ^3\Sigma_u^+)$ and $N_2(a'\ ^1\Sigma_u^-)$. These states are the energy reservoirs that account for the reactivity of nitrogen plasmas. $N_2(X\ ^1\Sigma_g^+, v)$ and $N_2(A\ ^3\Sigma_u^+)$ molecules are very significant in the production of the radiative state $N_2(B\ ^3\Pi_g)$, which gives rise to the strongest emission bands $N_2(B\ ^3\Pi_g \rightarrow A\ ^3\Sigma_u^+)$ in a nitrogen

[a] e-mail: vguerra@alfa.ist.utl.pt

discharge, known as the first positive system of N_2. Collisions between two $N_2(A\ ^3\Sigma_u^+)$ molecules can also produce N_2 molecules in higher electronic states, such as $N_2(B\ ^3\Pi_g)$ and $N_2(C\ ^3\Pi_u)$. The metastable species $N_2(A\ ^3\Sigma_u^+)$ and $N_2(a'\ ^1\Sigma_u^-)$ also play a major role in Penning ionization within a discharge, whereas $N_2(X\ ^1\Sigma_g^+, v)$ and $N_2(A\ ^3\Sigma_u^+)$ molecules are essential to understand dissociation and gas heating. $N_2(X\ ^1\Sigma_g^+, v)$ molecules, in levels as high as $\sim$35, are crucial as well to realize what are the mechanisms responsible for the enhancement of the light emissions observed in the short-lived afterglow, namely of the emission bands of the first positive $N_2(B\ ^3\Pi_g \rightarrow A\ ^3\Sigma_u^+)$, second positive $N_2(C\ ^3\Pi_u \rightarrow B\ ^3\Pi_g)$ and first negative $N_2^+(B\ ^2\Sigma_u^+ \rightarrow X\ ^2\Sigma_g^+)$ systems of N_2.

Another motivation to write this article is to review the crucial results and stress the approximations usually made. However, we should keep in mind that the current understanding of nitrogen plasmas relies in the available collision data. And, as we shall see, this data is far from being well known.

In this work we will analyse stationary nitrogen discharges, produced either by direct-current or a microwave structure, operating at pressures close to 1 torr, in cylindric geometry. The structure of the paper is the following. Section 2 is dedicated to the discharge. We will review the main results known concerning each of the relevant kinetics, and point out how they are interconnected. Section 3 is devoted to the afterglow. In this section, more than just a review, we will present some recent results, related to the effects of electron superelastic collisions with $N_2(A\ ^3\Sigma_u^+)$ and to the possibility of electron mediated vibrational to electronic (V-E) energy transfers. Finally, the main results will be summarized in Section 4.

2 Stationary discharges

In this section we make a survey of low-pressure stationary nitrogen discharges. We discuss the different kinetics and point out how the pivot ensuring a strong link between them is the vibrational distribution function of ground-state nitrogen molecules. The very important mechanisms of excitation of electronic states, dissociation, ionization and gas heating are examined in detail.

2.1 Electron kinetics

The first step in the modelling of stationary discharges is to describe the electron kinetics. Electrons gain energy from the electric field and subsequently redistribute it among the atomic and molecular internal degrees of freedom, dissociation and ionization. These processes of gain and loss of electron energy are adequately described by the electron Boltzmann equation, which can be solved by several techniques. The most common include the two-term expansion of the electron distribution in spherical harmonics, multi-term expansions, and Monte Carlo methods.

We shall concentrate our attention in the two-term expansion, since it allows a computationally straightforward coupling to other kinetics. It provides accurate enough results for discharge modelling, being the meaning of "accurate" discussed below. The two-term expansion is widely used in low-temperature plasma studies, and the resulting homogeneous electron Boltzmann equation takes the form [1,2]

$$\frac{dG}{du} = \sum_{i,j} \left[\sqrt{u + u_{ij}}\ \nu_{ij}(u + u_{ij})\ f(u + u_{ij}) - \sqrt{u}\ \nu_{ij}\ f \right.$$
$$\left. + \sqrt{u - u_{ij}}\ \nu_{ji}(u - u_{ij})\ f(u - u_{ij}) - \sqrt{u}\ \nu_{ji}\ f \right]. \quad (1)$$

Here, $f(u)$ is the electron energy distribution function (EEDF), obeying to the normalization condition $\int_0^\infty f \sqrt{u}\ du = 1$, where $u = \frac{1}{2}mv^2$ is the electron energy. Once the EEDF is known, the rate constants for each electron-heavy particle collision process $i \rightarrow j$ are readily calculated from

$$C_i^j = \sqrt{\frac{2}{m}} \int_0^\infty u\ \sigma_{ij}(u)\ f(u)\ du, \quad (2)$$

with σ_{ij} denoting the corresponding cross-section.

The terms inside the brackets on the right-hand side of equation (1) take into account the effects of excitation of vibrational and electronic states of N_2 by inelastic collisions (the first and second terms) and of de-excitation of vibrational states by electron superelastic collisions (the third and forth terms), with u_{ij}, ν_{ij} and ν_{ji} denoting the energy threshold and the inelastic and superelastic collision frequencies, respectively. $G(u)$ represents the total electron flux in energy space due to the continuous terms in the Boltzmann equation. $G(u)$ is given by the sum of the fluxes driven by the applied HF or DC field, G_E; the elastic collisions, G_c; the electron-electron ($e-e$) collisions, G_{e-e}; and the inelastic and superelastic collisions of electrons with rotational levels assuming a continuous approximation, G_{rot}. These terms can be written, respectively, in the forms [1,2]

$$G_E = -\frac{(eE)^2}{3m\ \nu_c^e}\ \frac{1}{1 + (\omega/\nu_c^e)^2}\ u^{3/2}\ \frac{df}{du}; \quad (3)$$

$$G_c = -\frac{2m}{M}\ \nu_c\ u^{3/2} \left(f + kT_g\ \frac{df}{du} \right); \quad (4)$$

$$G_{e-e} = -\ 2\ \nu_{e-e}\ u^{3/2} \left(I(u)\ f + J(u)\ \frac{df}{du} \right); \quad (5)$$

$$G_{rot} = -\ 4\ B\ \nu_0\ \sqrt{u}\ f. \quad (6)$$

In these equations, ω is the field frequency, E is the DC electric field field or its rms for a microwave field ($E_0/\sqrt{2}$, with E_0 being the field amplitude), ν_c^e is an effective collision frequency for momentum transfer including both elastic and inelastic contributions [3], ν_c is the elastic electron-neutral collision frequency for momentum transfer, M is the molecular mass, T_g is the gas temperature, ν_{e-e} is the

electron-electron collision frequency given by [1]

$$\nu_{e-e} = 4\pi \left(\frac{e^2}{4\pi\epsilon_0 m}\right)^2 \frac{\ln \Lambda}{v^3} n_e , \qquad (7)$$

with ϵ_0 denoting the vacuum permittivity and $\ln \Lambda$ the Coulomb logarithm, I are J integral functions of $f(u)$ known as Spitzer's integrals and given by [1]

$$I(u) = \int_0^u f(u) \sqrt{u} \, du \qquad (8)$$

and

$$J(u) = \frac{2}{3} \left(\int_0^u f(u) \, u^{3/2} \, du + u^{3/2} \int_u^\infty f(u) \, du\right). \quad (9)$$

Furthermore, $B(= 2.5 \times 10^{-4}$ eV$)$ is the rotational constant in N_2, and $\nu_0 = n_0 \sqrt{2u/m} \, \sigma_0$ is a frequency for rotational exchanges induced by electron impact, including both inelastic and superelastic processes, obtained using the continuous approximation [2], in which n_0 is the gas density and $\sigma_0 = 8\pi q^2 a_0^2/15$, with q $(=1.01$ in $N_2)$ denoting the electric quadrupole moment in units of ea_0^2 and a_0 the Bohr radius.

The validity of the two-term approximation has been questioned very recently [4]. None of the remarks made in that work is very important for discharge modeling under the conditions of this study, since the range of variation of the reduced electric field, E/N, is very narrow (from $\sim 3 \times 10^{-16}$ to 1.5×10^{-15} V.cm^2). Nevertheless, we shall review now some of the approximations usually made.

In equation (1) ionization is treated as any other excitation process, with a single energy loss equal to the ionization energy, neglecting the production of new electrons. Under discharge conditions, the effect of secondary electron collisions is negligible in N_2 for $E/N \leq 3 \times 10^{-15}$ V.cm^2, as it was shown in [5]. The very small effect of the assumptions related to the treatment of ionization in the calculated EEDF was more recently confirmed in [6], in calculations performed for a Ne/Xe/HCl mixture.

The continuous approximation for the rotational cross-sections was investigated in [7]. It was concluded it yields results accurate to within a few percent for values of the characteristic energy, u_k, larger than 0.046 eV ($u_k = eD/\mu$, where e is the electronic charge, D is the diffusion coefficient and μ is the mobility).

The most serious remark that can be done is to know if the conditions of "small anisotropies" intrinsic to the two-term expansion are true. In particular, nitrogen cross-sections violate one of the assumptions of the technique, in virtue of the large low-energy vibrational excitation cross-section. This cross-section peaks at electron energies of about 2 eV, becoming an important fraction of the sum of the momentum transfer cross-sections. A comprehensive study of the validity of two-term approximation was done in the milestone works of Pitchford and Phelps [3,8]. The errors resulting from the use of the two-term expansion in the most unfavorable case, which corresponds to the presence of many electrons with energies on the region of

the maximum of the vibrational excitation cross-section, at $E/N \simeq 7 \times 10^{-16}$ V.cm^2, are, approximately, 1, 5 and 30% for the drift velocity, the transverse diffusion coefficient, and the electronic excitation coefficients, respectively. These errors may be considered acceptable in discharge modeling, but the situation is actually better than that. The question is that the electron cross-sections used in two-term calculations do *not* have to be the most accurate experimentally determined cross-sections available. They form in fact an operative set carefully adjusted to ensure good results when used in two-term codes.

Equation (1) assumes that the EEDF is everywhere in equilibrium with the local electric field. The non local approach was developed in [9,10] and reviewed in [11]. A rough criterium for locality is when the electron energy relaxation length is much shorter than the spatial characteristic length, which sets a minimum value of pressure for the domain of validity of the local approximation. For nitrogen surface-wave discharges, which exhibit a characteristic axial inhomogeneity [12], the local regime was verified to occur at least for pressures above 0.5 torr [13,14].

For alternating fields, such as in a microwave discharge, the effective field approximation can be used whenever $\omega \gg \nu_e$, where ν_e is the energy relaxation frequency. In this case, the time modulation of the EEDF is strongly reduced [15]. Moreover, if the frequency ν_c^e is independent of the electron energy, the EEDF can be obtained by solving the Boltzmann equation in a DC field, with an effective field strength given by

$$E_{eff} = \frac{E_0}{\sqrt{2}} \frac{\nu_c^e}{[\omega^2 + (\nu_c^e)^2]^2}. \qquad (10)$$

The effective field approximation has been extended to situations where ν_c^e depends on the electron energy by replacing in equation (10) ν_c^e by a momentum transfer collision frequency for the bulk electrons which can be somewhat arbitrarily chosen [16,17].

Another simplification usually introduced in solving equation (1) is to treat the excitation of electronic states as a single energy loss process assuming that all the molecules are in the ground vibrational level $N_2(X, v = 0)$. The effect of considering individual $N_2(X, v - Y, v')$ transitions has been studied in [18–20]. The influence of excitation from vibrationally excited states can be relatively important, specially at low values of E/N.

Of course the choice of the cross-sections to be used in the electron Boltzmann equation is of great importance. Our cross-section set is largely based on the one developed by Pitchford and Phelps [21,22] for a two-term code, with a few additions described in detail in [23]. Table 1 lists the collision processes between electrons and N_2 molecules taken into account in the calculation of the EEDF from equation (1).

One important issue is the choice of the cross-sections for transitions between vibrationally excited levels (see B14 in Tab. 1). The set from [21,22] includes only the excitation of levels $w = 1, \ldots, 8$ from $v = 0$. For the cross-sections for excitation of levels w from $v > 0$, we assume an identical shape and magnitude with the

Table 1. Processes involving N_2 molecules considered in the Boltzmann equation (1).

B1	$e + N_2 \longrightarrow e + N_2$
B2	$e + N_2(X, v=0) \longrightarrow e + N_2(A\ ^3\Sigma_u^+)$
B3	$e + N_2(X, v=0) \longrightarrow e + N_2(B\ ^3\Pi_g)$
B4	$e + N_2(X, v=0) \longrightarrow e + N_2(W\ ^3\Delta_u)$
B5	$e + N_2(X, v=0) \longrightarrow e + N_2(B'\ ^3\Sigma_u^-)$
B6	$e + N_2(X, v=0) \longrightarrow e + N_2(a'\ ^1\Sigma_u^-)$
B7	$e + N_2(X, v=0) \longrightarrow e + N_2(a\ ^1\Pi_g)$
B8	$e + N_2(X, v=0) \longrightarrow e + N_2(w\ ^1\Delta_u)$
B9	$e + N_2(X, v=0) \longrightarrow e + N_2(C\ ^3\Pi_u)$
B10	$e + N_2(X, v=0) \longrightarrow e + N_2(E\ ^3\Sigma_g^+)$
B11	$e + N_2(X, v=0) \longrightarrow e + N_2(a''\ ^1\Sigma_g^+)$
B12	$e + N_2(X, v=0) \longrightarrow e + N_2(\text{upper singlets})$
B13	$e + N_2(X, v=0) \longrightarrow e + e + N_2{}^+$
B14	$e + N_2(X, v=0, \ldots, 9) \rightleftharpoons e + N_2(X, w=v+1, \ldots, 10)$

Fig. 1. EEDFs calculated for a DC field with $E/N = 3 \times 10^{-16}$ V.cm^2 (A) and 7×10^{-16} V.cm^2 (B), for $T_V = T_g = 300$ K (—) and $T_V = 5000$ K (– –).

cross-section for the transition $0 \rightarrow (w - v)$, but with a different energy threshold accounting for the anharmonicity of the oscillator. A comparison of this procedure with other hypotheses has been performed in [24], suggesting the correctness of the present approach. Nevertheless, there are no certitudes for the best choice of cross-sections for electron collisions involving transitions between vibrational levels, and this is presently a subject of research. For example, a study of the effect of these cross-sections on the calculated electron temperatures in the nitrogen afterglow has recently been done in [25]. It is also worth to mention the semi-empirical theory developed in [26], which has provided a new cross-section set for the transitions between vibrationally excited levels. The influence of these newer cross-sections in the modeling of nitrogen discharges is now under investigation [27].

As mentioned above, the cross-section for excitation of the manifold of vibrational levels is very high in N_2. Consequently, the energy transfer from electrons to vibrations is very effective, and the vibrational levels play a central role in nitrogen plasmas. The fractional power transferred by the electrons into vibrational excitation was quantified in [23], easily overcoming 50%, depending on the value of E/N and the degree of vibrational excitation. Since ground-state vibrationally excited $N_2(X\ ^1\Sigma_g^+, v)$ molecules are strongly populated, electron inelastic and superelastic collisions with these molecules must be taken into account in the Boltzmann equation. The necessity to know the vibrational distribution function (VDF) of ground-state molecules,

$$\delta_V = [N_2(X\ ^1\Sigma_g^+, v)]/[N_2], \qquad (11)$$

to solve the electron Boltzmann equation (1) clearly shows the strong coupling between vibration and electron kinetics. Some hypotheses usually made to solve the Boltzmann equation decoupled from the vibrational kinetics are to consider VDFs according to Boltzmann, Treanor [28] or Gordiets [29] distributions, but they lead to large errors in certain circumstances. The interplay between electron
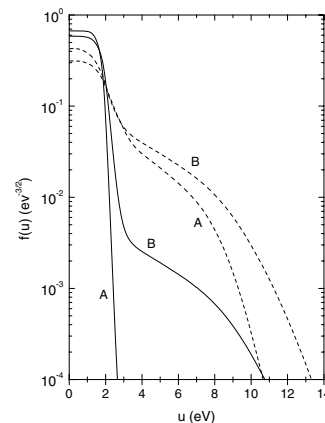
and vibrational kinetics was investigated in a series of papers by Capitelli and co-workers [19,30,31] and in our group [15,20,23,32], and will be further discussed in Section 2.2. The most decisive effect in the calculated EEDF results from superelastic collisions. They cause a significant enhancement of the high-energy tail of the EEDF, which becomes more pronounced as the vibrational excitation increases, as it has been first pointed out in [33] and can be seen in Figure 1. Superelastic collisions are always very important for all values of the reduced electric field considered in this paper, becoming less important as E/N increases.

Since superelastic collisions of electrons with vibrationally excited molecules are so important, it is natural to wonder if superelastic collisions with electronically excited states can modify the EEDF as well. The first electronic metastable state of nitrogen is $N_2(A\ ^3\Sigma_u^+)$, with an energy threshold of about 6.2 eV. Under stationary discharge conditions, it is the most populated electronic metastable state. The effect of superelastic collisions with $N_2(A\ ^3\Sigma_u^+)$ has been studied systematically in [31,34,35]. It has been shown that this effect can be important only when the degree of vibrational excitation is very low, practically disappearing for $\Theta_1 \geq 4000$ K, with Θ_1 denoting the characteristic $0-1$ vibrational temperature of N_2. This can be achieved only with very low residence times in a discharge [31]. As the vibrational excitation become important, the electron superelastic collisions with $N_2(X\ ^1\Sigma_g^+, v)$ molecules mask the effect. Superelastic collisions with $N_2(A\ ^3\Sigma_u^+)$ can be important in the afterglow, again for conditions of low vibrational excitation, as calculated in [24,25]. To have a quantitative idea of the importance of this effect in stationary discharges, Table 2 shows the calculated electron excitation rate coefficients of states $N_2(A\ ^3\Sigma_u^+)$ and $N_2(B\ ^3\Pi_g)$, for a reduced electric field $E/N \simeq 5 \times 10^{-16}$ V.cm^2, vibrational temperature $T_V \simeq 6200$ K, and field frequency $f = 433$ MHz. Here, T_V is the characteristic vibrational temperature of the modified Treanor-like distribution that best fits the fractional populations in the lowest four vibrational levels. This set

Table 2. Calculated electron excitation rate coefficients of states $N_2(A\ ^3\Sigma_u^+)$ (C_X^A) and $N_2(B\ ^3\Pi_g)$ (C_X^B), as a function of the fractional concentration of the state $A\ ^3\Sigma_u^+$, taking into account superelastic collisions with this state, for $E/N \simeq 5 \times 10^{-16}$ V.cm^2, $T_V \simeq 6200$ K and $f = 433$ MHz (see text).

$[N_2(A)]/N$	C_X^A (cm^3/s)	C_X^B (cm^3/s)
0	3.24×10^{-11}	2.89×10^{-11}
10^{-5}	3.24×10^{-11}	2.89×10^{-11}
10^{-4}	3.24×10^{-11}	2.90×10^{-11}
10^{-3}	3.28×10^{-11}	2.94×10^{-11}
10^{-2}	3.69×10^{-11}	3.41×10^{-11}

of parameters corresponds to the operating conditions of the discharge to be analysed in Section 3. Table 2 shows that superelastic collisions with $N_2(A\ ^3\Sigma_u^+)$ may become important when the relative population of this state is bigger than 10^{-2}. As we shall see in Section 2.3, this is very unlikely to occur for the discharge conditions analysed in this work, and they can usually be neglected.

The degree of dissociation in low-pressure nitrogen discharges is usually relatively low. Nevertheless, electron collisions with N atoms should be taken into account in the Boltzmann equation when $[N]/N \gtrsim 10^{-3}$ [36,37]. For this reason we have solved the electron Boltzmann equation (1) for a mixture N_2-N, taking into account the electron cross-section for momentum transfer of $N(^4S)$ atoms and the excitation of the metastable states $N(^2D)$ and $N(^2P)$ from ground state $N(^4S)$ atoms. It is straightforward to write the Boltzmann equation for a mixture of gases. Its final form can be found in [38]. Electron collisions with atoms correspond to another direct coupling of electron and heavy-particle kinetics: it is necessary to know the fractional atomic concentration in order to calculate the EEDF, but it is also necessary to know the EEDF to calculate the atomic concentration.

Electron-electron (e-e) collisions can often be neglected. They tend to bring the EEDF to a Maxwellian distribution, which can be significantly modified for high degrees of ionization, $\delta_e = n_e/N$, typically $\delta_e \gtrsim 10^{-4}$ [39,40]. As it will be shown in Section 3, e-e collisions can be important in the afterglow at much lower ionization degrees.

The procedure to numerically solve equation (1) is detailed in [41], in the absence of e-e collisions. These can be included in a similar way, but the non-linearity of the resulting discrete equations eforces an iterative procedure. The iterations can be made to converge very quickly, if we use the physical condition that the total power loss by electrons through e-e collisions must be zero.

The solution of the electron Boltzmann equation provides detailed information about the EEDF and all electron transport parameters and excitation rate coefficients. The two-term approximation is not at all computationally heavy. It can hence be used in self-consistent codes, even if an iterative procedure between the electron and the heavy-particle kinetics modules is necessary (to update the population of vibrational levels and nitrogen atoms, or the
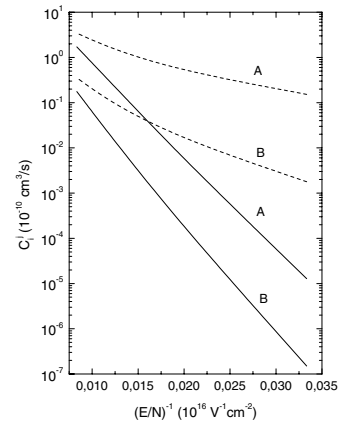

Fig. 2. Calculated electron rate coefficient for excitation of state $B\ ^3\Pi_g$ (A) and for dissociation (B), for $T_V = 500$ K (—) and 5000 K (– –).

value of the reduced electric field, for example). Nevertheless, if the EEDF is not absolutely needed, for discharge modeling it is possible to find approximate expressions for the different excitation rate coefficients (2). In the absence of vibrational excitation, they can be well approximated by expressions of the type

$$\log C_i^j = -a - b(E/N)^{-1}, \qquad (12)$$

where a and b are constants [42]. More accurate expressions, valid for a wide range of values of T_V, where obtained in [43]. Figure 2 shows the rate coefficients for excitation of state $N_2(B\ ^3\Pi_g)$ and for dissociation, as a function of $(E/N)^{-1}$, in the absence (full curves) and presence (dashed curves) of vibrational excitation. The relatively unusual chosen axis allow the direct determination of coefficients a and b in the expression (12).

2.2 Vibrational kinetics

The vibrational levels of ground-state $N_2(X\ ^1\Sigma_g^+, v)$ molecules play a central role in nitrogen discharges and afterglows. As we have already seen in the previous section, the vibrational distribution function (11) strongly determines the shape of the EEDF. This is due not only to the strong cross-section for electron losses in the excitation of vibrational levels but also to superelastic collisions (cf. Fig. 1). Furthermore, several vibrational levels are involved in heavy-particle reactions, some of them leading to dissociation, as we will see in Section 2.3.

The VDF can be calculated from the solution of the rate balance equations for the creation and loss of the various vibrational levels. The different processes to be taken into account include electron-vibration (e-V), vibration-vibration (V-V), vibration-translation (V-T), vibration-electronic (V-E) energy exchanges, as well as deactivation at the wall and chemical reactions, the later including dissociation and recombination. Table 3 lists the different mechanisms considered here, with D denoting dissociation and W wall processes. Notice that for V-V and V-T

Table 3. Kinetics of $N_2(X\ {}^1\Sigma_g^+$, v = 0−45) molecules.

e-V	$e + N_2(X, v) \rightleftharpoons e + N_2(X, w)$
V-V	$N_2(X, v) + N_2(X, w) \rightleftharpoons N_2(X, v - 1) + N_2(X, w + 1)$
V-T N_2-N_2	$N_2(X, v) + N_2 \rightleftharpoons N_2(X, v - 1) + N_2$
V-T N_2-N	$N_2(X, v) + N \rightleftharpoons N_2(X, w) + N$
	$N_2(X, v) + N \rightleftharpoons N + N_2(X, w)$
Wall	$N_2(X, v) + \text{wall} \rightarrow N_2(X, v - 1)$
e-D	$e + N_2(X, v) \rightarrow e + N + N$
V-D	$N_2(X, v) + N_2(X, w = 45) \rightarrow N_2(X, v - 1) + N + N$
	$N_2 + N_2(X, w = 45) \rightarrow N_2 + N + N$
Chemistry	See Table 5

reactions we have only considered single-quantum transitions, which are the most likely ones, except for V-T exchanges in the system N_2-N. This later case includes both a direct process and a reactive one, in which an atomic exchange between the two collision partners takes place. The entry "chemistry" designates all reactions involving the creation or destruction of any vibrational level, such as V-E, recombination, and dissociation from levels other than the last bound vibrational level, $v = 45$. Examples of these processes are reactions C2–C6 from Table 5. Dissociation by V-V and V-T processes, known as *vibrational dissociation*, is modelled as a transition from $v = 45$ to a pseudo-level in the continuum [19].

The rate balance equation for the concentration of each vibrational level, n_v, can then be written as

$$
\begin{aligned}
\frac{dn_v}{dt} &= n_e \sum_{w \neq v} n_w C_w^v - n_e n_v \sum_{w \neq v} C_v^w \\
&+ n_{v-1}[N_2] P_{v,v-1} + n_{v+1}[N_2] P_{v+1,v} \\
&- n_v \left(P_{v,v-1} + P_{v,v+1} \right) + [N] \sum_{w \neq v} n_w P_{w,v}^{N_2-N} \\
&- n_v[N] \sum_{w \neq v} P_{v,w}^{N_2-N} + n_{v-1} \sum_w n_{w+1} Q_{v-1,v}^{w+1,w} \\
&+ n_{v+1} \sum_w n_w Q_{v+1,v}^{w,w+1} \\
&- n_v \left(\sum_w n_{w+1} Q_{v,v+1}^{w+1,w} + \sum_w n_w Q_{v,v-1}^{w,w+1} \right) \\
&- \nu_W(v) n_v + \text{Chem}(v).
\end{aligned}
\tag{13}
$$

Here, n_e, $[N_2]$ and $[N]$ are the electron, molecular and atomic densities, respectively, C, P and Q denote the rate coefficients for e-V, V-T and V-V processes, respectively, $\nu_W(v)$ is the loss frequency of $N_2(X, v)$ molecules to the wall, and $\text{Chem}(v)$ is the rate of change of the concentration n_v due to the heavy-particle reactions listed in Table 5. For steady-state conditions, this set of equations can be solved directly imposing $dn_v/dt = 0$.

Equation (13) shows unambiguously the strong link between the different kinetics. First, electrons determine the energy input into the vibrational mode, expressed by the excitation coefficients C_v^w. This energy is redis-

tributed among the vibrational manifold through V-V and V-T processes. Surface kinetics directly affects vibrations, both due to its strong influence in the atomic concentration $[N]$ (which noticeably affects the VDF via V-T N_2-N exchanges) and to the direct deactivation of vibrationally excited levels at the wall. Finally the resulting VDF will have a strong impact in the neutral and charged particle chemistry, as we will see in the next section.

As we have mentioned in the previous section, the mutual action of electron and vibrational kinetics in gas discharges has been studied systematically in a series of papers from the 80 s. However, the study of the time evolution of the VDF, in conditions where the electron kinetics is not determinant, is an important issue in atmospheric chemistry and hypersonic flows for aerospace applications.

A decisive step to obtain realistic populations of vibrationally excited molecules in different levels is the choice of the collisional data in equation (13). There are different theories allowing the calculation of the V-V and V-T rate coefficients in N_2-N_2 collisions, such as SSH (Schwartz, Slawsky and Herzfeld) theory [75,76], later on modified in [77,78], or the forced harmonic oscillator [79,80]. This later model is in good agreement with the three-dimensional semiclassical trajectory calculations of Billing and Fisher [81], which stand as a benchmark for the N_2-N_2 V-V and V-T rate coefficients. The correctness of the coefficients from [81] has been suggested in several independent studies [37,82,83], so that they are used in this work.

The rate coefficients $P_{v,w}^{N_2-N}$ for the V-T collisions in the system N_2-N are still poorly known. They have been firstly calculated in [84,85], for a large number of reactions. We used these values in some of our previous investigations [86,48]. New calculations, reporting slightly weaker coefficients, were presented in [87,88] and were used in [89,49]. We have approximated the new values by

$$
P_{v,v-1}^{N_2-N} = A_0 \exp\left(-\frac{A_1}{v} + \frac{A_2}{v^2} \right),
\tag{14}
$$

where the constants A_0, A_1 and A_2 are given in Table 4, both for the reactive and non-reactive collisions. We considered the non-reactive coefficient to be zero for $v < 9$ and the reactive one to vanish for $v < 7$. We have further assumed that $P_{v,w<v} = P_{v,v-1}$ if $v-w \leq 5$ and $P_{v,w<v} = 0$

Table 4. Constant coefficients to be used in expression (14). T_g is the gas temperature in K.

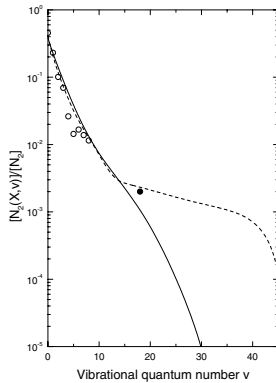|	Reactive	Non-reactive
A_0	$2.21 \times 10^4 / T_g^{1.43}$	$9.24 \times 10^4 / T_g^{1.63}$
A_1	$3.21 \times 10^4 / T_g^{0.80}$	$1.82 \times 10^4 / T_g^{0.70}$
A_2	$2.50 \times 10^5 / T_g^{1.04}$	$9.89 \times 10^3 / T_g^{0.44}$

Fig. 3. VDF of $N_2(X\ ^1\Sigma_g^+)$ molecules for a microwave discharge at $p = 3.3$ torr (—) and a DC discharge with $I = 20$ mA and $p = 0.5$ torr (– –). The experimental points correspond to the measurements reported in [93] (○) and [94] (●) (see text).

otherwise. Actually 5 quanta transitions are about a factor of two weaker than one quantum transitions, whereas transitions of 10 quanta are already one order of magnitude lower, as it is shown in [90]. In this last reference the calculations from [87,88] have been improved by considering a system of 67 vibrational levels, instead of just the 45 bound ones. The new values differ from the older ones only for gas temperatures $T_g > 2000$ K, so that no corrections need to be taken into account in the conditions of this study. However, our recent investigation in the nitrogen afterglow strongly suggests that the rate coefficients $P_{v,w}$ here described are still too strong, and we felt a need to somewhat reduce them in [50,91]. A rough estimation has determined that these coefficients should be reduced by a factor of five. We will return to this question in Section 3.

For the wall deactivation of $N_2(X\ ^1\Sigma_g^+, v)$ molecules at the wall (Pyrex surface) we have assumed a first-order mechanism and single-quantum transitions with a constant probability $\gamma_W = 4.5 \times 10^{-4}$ [92].

Figure 3 shows the calculated VDF for the same conditions as in Table 2, $E/N \simeq 5 \times 10^{-16}$ V.cm^2, $T_V \simeq 6200$ K, $f = 433$ MHz, gas temperature $T_g = 1000$ K, tube radius $R = 1.9$ cm, pressure $p = 440$ Pa, electron density $n_e = 3 \times 10^{10}$ cm^{-3} and relative atomic concentration $[N]/N \simeq 10^{-2}$ (full curve). Of course that only few of these quantities are independent, the others being calculated from the self-consistent model (see Sect. 2.5). The open circles are the Raman scattering measurements in the afterglow of a microwave discharge corresponding to the conditions of the calculations, for an afterglow time $t \simeq 1.5 \times 10^{-2}$ s [93]. As it will be shown in Section 3, the population of these low vibrational levels for this af-

terglow time is practically the same as in the discharge. The black circle is the cavity ringdown spectroscopy measurement of the population of level $v = 18$ in a DC discharge at $p = 2.3$ torr and $I = 100$ mA [94], which is, to our knowledge, the only measurement available for a relatively high vibrational level. The VDF has a characteristic shape, resulting from the combined effect of e-V and V-V exchanges at low vibrational levels, near resonant V-V exchanges at intermediate levels, which tend to form a plateau in this region, and V-T exchanges with N_2 molecules and N atoms at the high levels. For these discharge conditions of relatively high excitation the plateau is drastically reduced and the population of the last bound vibrational level, $v = 45$, is extremely low. Therefore, vibrational dissociation cannot possible occur. Dissociation by a pure vibrational mechanism can take place in a stationary discharge only in conditions of simultaneously low values of the gas temperature and the degree of dissociation, which can eventually be met in a DC discharge operating at low discharge currents. The dashed curve in Figure 3 corresponds to the quite favorable case of a DC discharge with $I = 20$ mA, $R = 0.75$ cm and $p = 0.5$ torr, for which we have $T_g \simeq 340$ K, $T_V = 4800$ K, $E/N = 11.5 \times 10^{-16}$ V.cm^2 and $[N]/N = 5.9 \times 10^{-3}$. The plateau at intermediate levels is now very extended. Even though, the ratio between the rates of vibrational and direct electron impact dissociation is only 0.34. This value is reduced to 0.02 when I raises to 80 mA, while it can significantly increase if we keep low currents and increase the gas pressure. However, in this later case other important sources of nitrogen atoms do exist, as it will be shown in the next section. Let us still recall we have reduced the rate coefficient for N_2-N V-T exchanges. If the actual rates are higher than ours, then the high levels of the VDF will be still less populated and vibrational dissociation will not occur in any circumstances.

2.3 Chemical kinetics

We turn now to the description of heavy-particles other than the vibrational levels of ground-state N_2 molecules, such as electronically excited states, atomic species and positive ions. First we discuss the chemistry of neutral species. Special attention will be paid to dissociation, since this is an important mechanism still poorly understood in discharge conditions. Next we review the reactions involving charged particles and the ionization processes. Finally, we consider the gas heating channels of relevance in nitrogen discharges.

2.3.1 Excited states

Nitrogen "chemistry sets" are of course very important in atmospheric and ionospheric physics, and in plasma chemistry in general. Several of these sets are available in the literature. A very complete and unavoidable one has been compiled by Kossyi and co-workers in [57]. Their kinetic scheme was built assuming gas temperatures between 220

Table 5. Nitrogen chemistry set.

	Process	Rate coefficient	Reference
C1	Diffusion of $N_2(A)$ to the wall	$ND = 5 \times 10^{18}\sqrt{\frac{T_g(\text{K})}{300}}$ cm^{-1}s^{-1}	[44]
C2	$N_2(A)+N_2(A) \rightarrow N_2(B)+N_2(X, v = 8)$	$k = 7.7 \times 10^{-11}$ cm^{3}s^{-1}	[45,46]
C3	$N_2(A)+N_2(A) \rightarrow N_2(C)+N_2(X, v = 2)$	$k = 1.5 \times 10^{-10}$ cm^{3}s^{-1}	[47,46]
C4	$N_2(A)+N_2(X, 5 \leq v \leq 14) \rightarrow N_2(B)+N_2(X, v = 0)$	$k = 2 \times 10^{-11}$ cm^{3}s^{-1}	[48]
C5	$N_2(A)+N_2(X, 14 \leq v \leq 19) \rightarrow N_2(X, v = 0)+N+N$	$k = 4.5 \times 10^{-11}\exp(-1765/T_g)$ cm^{3}s^{-1}	[49,50]
C6	$N_2(A)+N(^4S) \rightarrow N_2(X, 6 \leq v \leq 9)+N(^2P)$	$k = 4 \times 10^{-11}$ cm^{3}s^{-1}	[51]
C7	$N_2(B)+N_2 \rightarrow N_2(A)+N_2$	$k = 0.95 \times 3 \times 10^{-11}$ cm^{3}s^{-1}	[52,48]
C8	$N_2(B)+N_2 \rightarrow N_2(X, v = 0)+N_2$	$k = 0.05 \times 3 \times 10^{-11}$ cm^{3}s^{-1}	[48,53]
C9	$N_2(B) \rightarrow N_2(A)+h\nu$	$\nu = 2 \times 10^5$ s^{-1}	[54]
C10	$N_2(C) \rightarrow N_2(B)+h\nu$	$\nu = 2.74 \times 10^7$ s^{-1}	[55]
C11	$N_2(B') \rightarrow N_2(B)+h\nu$	$n_e[N_2(X)]C_X^{B'}$	
C12	Diffusion of $N_2(a')$ to the wall	as for $N_2(A)$	
C13	$N_2(a')+N_2 \rightarrow N_2(B)+N_2$	$k = 1.9 \times 10^{-13}$ cm^{3}s^{-1}	[56,57]
C14	Diffusion of $N_2(a)$ to the wall	as for $N_2(A)$	
C15	$N_2(a)+N_2 \rightarrow N_2(a')+N_2$	$k = 2.0 \times 10^{-11}$ cm^{3}s^{-1}	[58]
C16	$N_2(a) \rightarrow N_2(X, v = 0)+h\nu$	$\nu = 1.8 \times 10^4$ s^{-1}	[58]
C17	$N_2(a) \rightarrow N_2(a')+h\nu$	$\nu = 1.91 \times 10^2$ s^{-1}	[59]
C18	Diffusion of $N_2(w)$ to the wall	as for $N_2(A)$	
C19	$N_2(w) \rightarrow N_2(a)+h\nu$	$\nu = 6.5 \times 10^2$ s^{-1}	[60]
C20	$N_2(w)+N_2 \rightarrow N_2(a)+N_2$	$k = 10^{-11}$ cm^{3}s^{-1}	[61]
C21	$N_2(a'')+N_2 \rightarrow$ (products)	$k = 2.3 \times 10^{-10}$ cm^{3}s^{-1}	[62]
C22	$e+N_2(A) \rightarrow e+N_2(B)$	$f(E/N)$	[63]
C23	$e+N_2(A) \rightarrow e+N_2(C)$	$f(E/N)$	[63]
C24	$e+N_2(X) \rightarrow e+N(^4S)+N(^4S)$	$f(E/N)$	[64]
C25	$e+N_2(X) \rightarrow e+N(^4S)+N(^2D)$	$f(E/N)$	[64]
C26	$e+N(^4S) \rightleftharpoons e+N(^2D)$	$f(E/N)$	[65]
C27	$e+N(^4S) \rightleftharpoons e+N(^2P)$	$f(E/N)$	[65]
C28	$e+N(^2D) \rightleftharpoons e+N(^2P)$	$f(E/N)$	[65]
C29	$2N_2(X, 10 < v < 25) \rightarrow N_2(X)+N+N$	$k = 3.5 \times 10^{-15}$ cm^{3}s^{-1}	[49]
C30	$N(^4S)+N(^4S)+N_2 \rightarrow N_2(B)+N_2$	$K = 8.27 \times 10^{-34}\exp\left(\frac{500}{T_g(\text{K})}\right)$ cm^{6}s^{-1}	[57]
C31	$N(^4S)+\text{Wall} \rightarrow \frac{1}{2}N_2(X, v = 0)$	$\gamma_d = 10^{-3}$; $\gamma_a = 3 \times 10^{-6}$ (see text)	[66,67]
C32	Diffusion of $N(^2D)$ to the wall	$ND = 6.4 \times 10^{18}\sqrt{\frac{T_g}{300}}$ cm^{-1}s^{-1}	[68]
C33	$N(^2D)+N_2 \rightarrow N(^4S)+N_2$	$k = 1 \times 10^{-13}\exp(-510/T_g)$ cm^{3}s^{-1}	[69]
C34	Diffusion of $N(^2P)$ to the wall	$ND = 5.2 \times 10^{18}\sqrt{\frac{T_g}{300}}$ cm^{-1}s^{-1}	[68]
C35	$N(^2P)+N(^4S) \rightarrow N(^4S)+N(^2D)$	$k = 6 \times 10^{-13}$ cm^{3}s^{-1}	[37]
C36	$N(^2P)+N(^4S) \rightarrow N(^4S)+N(^4S)$	$k = 1.8 \times 10^{-12}$ cm^{3}s^{-1}	[37]
C37	$N(^2P)+N_2 \rightarrow N(^4S)+N_2$	$k = 6 \times 10^{-14}$ cm^{3}s^{-1}	[37]
C38	$N(^2P)+N(X, v \geq 10) \rightarrow N(^4S)+N_2(A)$	$k = 10^{-10}\exp(-1300/T_g)$ cm^{3}s^{-1}	[37]
C39	$N_2(X, v \geq 39)+N(^4S) \rightarrow N_2(A)+N(^2D)$	$k = 10^{-11}$ cm^{3}s^{-1}	[50]
C40	$N_2(X, v \geq 38)+N(^4S) \rightarrow N_2(a')+N(^4S)$	$k = 10^{-11}$ cm^{3}s^{-1}	[50]
C41	$N_2(A)+N_2(a') \rightarrow e+N_4^+$	$k = 10^{-11}$ cm^{3}s^{-1}	[48]
C42	$N_2(a')+N_2(a') \rightarrow e+N_4^+$	$k = 5 \times 10^{-11}$ cm^{3}s^{-1}	[48]
C43	$e+N_2(A) \rightarrow e+e+N_2^+(X)$	$f(E/N)$	[70]
C44	$e+N_2(a') \rightarrow e+e+N_2^+(X)$	$f(E/N)$	[63]
C45	$e+N_2(B) \rightarrow e+e+N_2^+(X)$	$f(E/N)$	[63]

Table 5. Continued.

C46	$e+N_2(a) \rightarrow e+e+N_2^+(X)$	$f(E/N)$	[63]
C47	$e+N_2(w) \rightarrow e+e+N_2^+(X)$	$f(E/N)$	[63]
C48	$N(^2D)+N(^2P) \rightarrow N_2^+(X)+e$	$k = 10^{-13}$ cm^{3}s^{-1}	[37]
C49	$e+N_2^+(X) \rightarrow N(^4S)+N(^4S)$	$\alpha = 4.8 \times 10^{-7}(300/T_e[K])^{0.5}$ cm^{3}s^{-1}	[57]
C50	$e+N_4^+ \rightarrow N_2(X,v=0)+N_2(X,v=0)$	$\alpha = 2 \times 10^{-6}(300/T_e[K])^{0.5}$ cm^{3}s^{-1}	[57]
C51	$N_4^++N_2 \rightarrow N_2^+(X)+N_2(X,v=0)+N_2$	$k = 2.1 \times 10^{-16} \exp(T_g/121)$ cm^{3}s^{-1}	[71]
C52	$N_2^+(X)+N_2+N_2 \rightarrow N_4^++N_2$	$K = 6.8 \times 10^{-29}(300/T_g)^{1.64}$ cm^{3}s^{-1}	[72]
C53	$N_2(X,v \geq 12)+N_2^+(X) \rightarrow N_2^+(B)+N_2(X,v-12)$	$k = 10^{-11}$ cm^{3}s^{-1}	[73,71]
C54	$N_2^+(B) \rightarrow N_2^+(X)+h\nu$	$\nu = 1.6 \times 10^7$ s^{-1}	[74]
C55	Ambipolar diffusion of electrons,		
	$N_2^+(X)$, $N_2^+(B)$ and N_4^+ to the wall		

and 500 K, in conditions of negligible vibrational excitation. It is a good starting point, but of course vibrational excitation is critical in nitrogen discharges and afterglows. Another important reference, this time with the discussion of a large number of reactions involving vibrationally excited $N_2(X\ ^1\Sigma_g^+,v)$ molecules, is Slovetskii's book [95].

Early attempts in our laboratory to couple the electron and neutral heavy-particle kinetics were performed in [96,97]. Tabulated electron rate coefficients were used together with a very simple kinetic scheme allowing the calculation of the population of $N_2(A\ ^3\Sigma_u^+,v')$ molecules. The VDF of nitrogen ground-state molecules was imposed. Later on the same approach was used to determine the concentrations $[N_2(B\ ^3\Pi_g,v')]$ [98].

The simultaneous solution of the electron Boltzmann equation (1), the master equation for vibrational levels (13) and the rate balance equations for the creation and destruction of the excited states $N_2(A\ ^3\Sigma_u^+)$, $N_2(B\ ^3\Pi_g)$ and $N_2(C\ ^3\Pi_u)$ was done in [31,99]. Finally, discharge models including rather complete chemistry sets (which considered more electronically excited states, dissociation and charged particles) where developed in [37,48,71]. In the last two of these references the electric field sustaining the discharge was also self-consistently calculated (see below).

Table 5 lists the reactions that, together with the processes from Tables 1 and 3, are considered in this work. It is a refinement of the chemistry set proposed in [48], with the improvements suggested in [49,61,91,100]. It allows the calculation of the concentrations of the electronically excited states $N_2(A\ ^3\Sigma_u^+, B\ ^3\Pi_g, C\ ^3\Pi_u, a'\ ^1\Sigma_u^-, a\ ^1\Pi_g, w\ ^1\Delta_u, a''\ ^1\Sigma_g^+)$, of the atomic species $N(^4S, {}^2D, {}^2P)$ and of $N_2^+(X\ ^2\Sigma_g^+)$, $N_2^+(B\ ^2\Sigma_u^+)$ and N_4^+ ions. We assume that all the destruction processes of state $N_2(B'\ ^3\Sigma_u^-)$ lead to the production of $N_2(B\ ^3\Pi_g)$. The state $N_2(W\ ^3\Delta_u)$, not included in Table 5, deserve a separate comment given below. This table includes some electron processes, whose coefficient is indicated to be a function of E/N. With the exception of reactions C26 and C27, we do not take into account these processes during the solution of the electron Boltzmann equation (1). The excitation rate coefficients are simply obtained by the appropriate integral of the calculated EEDF over the corresponding cross-section.

The two values for the probability of atomic recombination C31, γ_d and γ_a, correspond to discharge and afterglow conditions, respectively (see Sect. 2.4). We believe this chemistry set to be adequate for the investigation of nitrogen discharges and afterglows in the conditions considered in this report. Of course other processes must be taken into account at different conditions. For example, the quenching of $N_2(C\ ^3\Pi_u)$ by N_2 molecules should be considered at higher pressures [101].
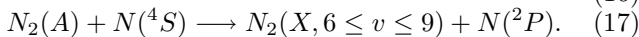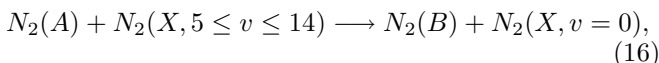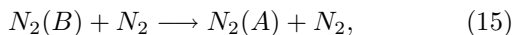
Once more, the choice and accuracy of the collisional data if of major importance. A vast collection of experimental and theoretical information on separate elementary reactions has been already accumulated. In spite of this, the question of whether the description of physicochemical phenomena on the basis of available kinetic schemes is satisfactory is permanently open. One relevant remark must be done to the possible temperature dependence of the various rate coefficients, since most of them have been measured at 300 K only. A second observation is that these are somehow "global" rate coefficients, since there is no discrimination of the vibrational levels of the electronically excited states. However, it is clear that the potential improvements obtained by taking into account a vibrational state-to-state scheme would immediately be lost due to the uncertainties in the respective collisional data.

We have assumed that all metastable states reaching the wall deactivate with unit probability (reactions C1, C12, C14, C18, C32 and C34). A slowly diffusing metastable state, which diffuses slower than $N_2(A\ ^3\Sigma_u^+)$ and with possible influence in the ionization growth during breakdown, was identified in [102,103]. These authors discuss a series of experiments suggesting that metastable reflection is not significant and rule out the $N_2(a'\ ^1\Sigma_u^-)$ state as the slowly diffusing state, suggesting highly vibrationally excited molecules, in levels $v = 27$–33. Nevertheless, a wall deactivation probability of only 10^{-3} was assumed for $N_2(a'\ ^1\Sigma_u^-)$ metastables in [104]. In what concerns the atomic metastables $N(^2D)$ and $N(^2P)$, we admit that, when they reach the wall, part of them is simply deactivated to the ground state $N(^4S)$, whereas the remaining part recombines into $N_2(X,v=0)$ molecules at the wall [100].

A relatively large list of reactions, such as the one in Table 5, may look uninteresting at first sight and even an attempt of obfuscation. However, we have tried to keep the number of processes to a minimum, as long as two conditions were satisfied. The first one is not to lose any physical insight. The mechanisms we have taken into account are almost all necessary to understand some particular issues of the nitrogen chemistry in the discharge and/or in the afterglow. In some of our previous works, already cited, we have focused our attention and discussed different subsets of the present chemistry scheme. The second condition is to obtain a closed system of equations. This is important if we want to perform self-consistent calculations, from example to avoid the need of using as input the concentration of one species. Having said this, it is clear that some reactions play a central role if we want to understand the general behavior of discharges and post-discharges in nitrogen. We will try now to go through Table 5 and stress some key features.

The first thing to retain is that the electronically excited molecular states are divided into the *triplet* and *singlet* manifolds, which practically do not interact with each other, although they are strongly coupled to the vibrational manifold and to the atomic states.

The triplet intrasystem cascading scheme involves the states $A\ ^3\Sigma_u^+$, $B\ ^3\Pi_g$, $W\ ^3\Delta_u$, $B'\ ^3\Sigma_u^-$ and $C\ ^3\Pi_u$. The different vibrational levels (B, v') and (W, v'') present close energy resonances, so that their populations are likely to be almost equilibrated in our pressure range [98,105]. Our model does not take into account directly the kinetics of $N_2(W\ ^3\Delta_u)$. However, it is considered indirectly in the kinetics of the $N_2(B\ ^3\Pi_g)$ state, since the collisional data measured in flow systems actually provide the relaxation coefficients for the coupled states as a whole rather than on the decay of the B or W states alone [45,105]. A strong collisional coupling of the same kind is believed to exist between different levels $N_2(A\ ^3\Sigma_u^+, v'')$ and $N_2(B\ ^3\Pi_g, v')$ [106], since $v'' = 7$ is near resonant with $v' = 0$. As mentioned before, such a detailed vibrational state-to-state kinetics seems at present a too ambitious project. Nevertheless, as it was pointed out in [48,107], the populations of $N_2(A\ ^3\Sigma_u^+)$, $N_2(B\ ^3\Pi_g)$ and nitrogen atoms, with the important participation of vibrationally excited molecules in low vibrational levels, are strongly coupled through reactions C4, C6 and C7 from Table 5, rewritten here:

$$N_2(B) + N_2 \longrightarrow N_2(A) + N_2, \qquad (15)$$

$$N_2(A) + N_2(X, 5 \leq v \leq 14) \longrightarrow N_2(B) + N_2(X, v = 0), \qquad (16)$$

$$N_2(A) + N(^4S) \longrightarrow N_2(X, 6 \leq v \leq 9) + N(^2P). \qquad (17)$$

The coupling with nitrogen atoms is reinforced with reaction C38,

$$N(^2P) + N_2(X, v \geq 10) \longrightarrow N(^4S) + N_2(A), \qquad (18)$$
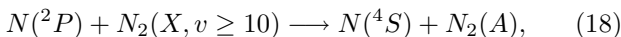
which was not considered in [48,107]. In order to quantify the strength of this coupling, Figure 4 shows the relative contribution of the different mechanisms of creation
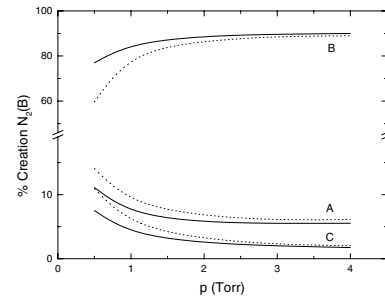

Fig. 4. Relative contribution of different mechanisms in the formation of $N_2(B\ ^3\Pi_g)$ molecules as a function of pressure, for a DC discharge with $R = 0.75$ cm and $I = 20$ mA (—) and $I = 80$ mA ($\cdots$): (A) $e+N_2(X) \rightarrow e+N_2(B)$; (B) $N_2(A)+N_2(X, 5 \leq v \leq 14) \rightarrow N_2(B)+N_2(X, v=0)$; and (C) $N_2(B', C) \rightarrow N_2(B)+h\nu$.

of $N_2(B\ ^3\Pi_g)$ molecules as a function of the gas pressure p, in a DC discharge in the conditions of reference [49] (S-52 glass cylindrical tube with inner radius $R = 7.5$ mm), for discharge currents $I = 20$ mA (full curves) and $I = 80$ mA (dotted curves). Curves A, B and C correspond, respectively, to the formation of $N_2(B\ ^3\Pi_g)$ by direct electron impact (process B3 in Tab. 1), from reaction (16), and as a consequence of the radiative decay of states $N_2(B'\ ^3\Sigma_u^-, C\ ^3\Pi_u)$ (processes C10 and C11). It is immediately seen that, for the conditions under analysis, $N_2(B\ ^3\Pi_g)$ molecules are essentially formed via reaction (16). The contribution of other processes not shown to the formation of $N_2(B\ ^3\Pi_g)$, such as the pooling reaction C2 or the intersystem crossing of $N_2(a'\ ^1\Sigma_u^-)$ C13, is always less than 2.5%. It is worth noting here that the intersystem crossing to produce $N_2(B\ ^3\Pi_g)$ is spin-allowed and can be near resonant for some vibrational levels. However, recent measurements reported in [108] indicate intersystem crossing to be large for collisions of $N_2(a'\ ^1\Sigma_u^-)$ with Xe, Kr, O_2 and NO, but small for N_2, H_2, CH_4 and Ar. That investigation shows that the yield of triplet nitrogen from the quenching of $N_2(a'\ ^1\Sigma_u^-, v = 0)$ by N_2 is less than 2%. The present results are practically not affected by considering the formation of $N_2(B\ ^3\Pi_g)$ in reaction C13 instead of other products. However, care must be taken for higher values of the pressure. Figures 5 and 6 show the relative contribution of several processes of creation and destruction of $N_2(A\ ^3\Sigma_u^+)$ molecules. With the same notation and for the same conditions as in Figure 4, the different curves in Figure 5 are for the creation of $N_2(A\ ^3\Sigma_u^+)$ metastables by radiative decay C9, $N_2(B) \rightarrow N_2(A) + h\nu$, curves A; quenching of $N_2(B\ ^3\Pi_g)$ (15), curves B; direct electron impact B2, $e+N_2(X) \rightarrow e+N_2(A)$, curves C; and excitation from $N_2(X\ ^1\Sigma_g^+)$ by atomic metastable impact (18), curves D. The different curves in Figure 6 correspond to destruction of $N_2(A\ ^3\Sigma_u^+)$ through processes (17), curves A; (16), curves B; C1, diffusion to the wall, curves C; pooling reactions C2 and C3, curves D. The behavior of the relative importance of the various mechanisms in Figures 4–6 is relatively easy to understand, keeping in mind a couple of things. First, the reduced electric field decreases with pressure (see below),
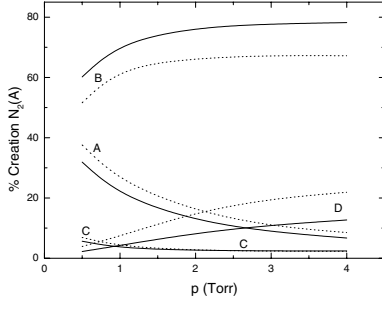
Fig. 5. Relative contribution of different mechanisms in the formation of $N_2(A\ ^3\Sigma_u^+)$ molecules as a function of pressure, for a DC discharge with $R = 0.75$ cm and $I = 20$ mA (—) and $I = 80$ mA ($\cdots$): (A) $N_2(B) \rightarrow N_2(A) + h\nu$; (B) $N_2(B) + N_2 \rightarrow N_2(A) + N_2$; (C) $e + N_2(X) \rightarrow e + N_2(A)$; and (D) $N(^2P) + N(X, v \geq 10) \rightarrow N(^4S) + N_2(A)$.
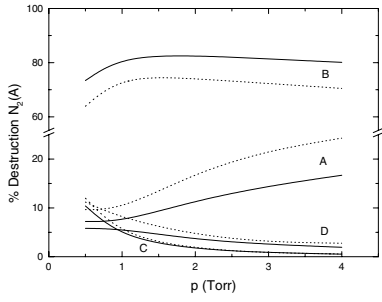

Fig. 6. Relative contribution of different mechanisms in the destruction of $N_2(A\ ^3\Sigma_u^+)$ molecules as a function of pressure, for a DC discharge with $R = 0.75$ cm and $I = 20$ mA (—) and $I = 80$ mA ($\cdots$): (A) $N_2(A) + N(^4S) \rightarrow N_2(X, 6 \leq v \leq 9) + N(^2P)$; (B) $N_2(A) + N_2(X, 5 \leq v \leq 14) \rightarrow N_2(B) + N_2(X, v = 0)$; (C) diffusion to the wall; and (D) $N_2(A) + N_2(A) \rightarrow N_2(B,C) + N_2(X, v)$.

which in turn leads to a decrease in the relative population of the electronically excited states with pressure (see Fig. 7). Second, for a fixed value of the discharge current the relative concentration of nitrogen atoms does not change too much in our pressure range, even slightly grows with p (see below). This justifies the raising importance of reactions (17) and (18) for the higher values of pressure. These figures show that $N_2(A\ ^3\Sigma_u^+)$ molecules are essentially "created from" and "destroyed forming" $N_2(B\ ^3\Pi_g)$. Therefore, the combined effect of reactions (15) and (16) do not constitute effective populating/depopulating mechanism for $N_2(A\ ^3\Sigma_u^+)$ and $N_2(B\ ^3\Pi_g)$ states, as these reactions just redistribute their populations among the triplet manifold. The same kind of argument can be used to some extent regarding reactions (17) and (18). In fact, the absolute populations of both triplet states are actually determined by other slower processes, such as reaction C8 of quenching of $N_2(B\ ^3\Pi_g)$ directly to the ground state and diffusion to the wall. The relative concentration of the three triplet states $N_2(A\ ^3\Sigma_u^+, B\ ^3\Pi_g, C\ ^3\Pi_u)$ is presented in Figure 7, together with the absorption measurements of $N_2(A\ ^3\Sigma_u^+)$ from [97] and the emission measurements of $N_2(B\ ^3\Pi_g)$ from [98]. Notice that the experiments in [97,98] were made in a tube of radius $R = 1$ cm.
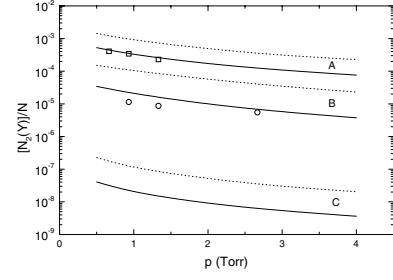

Fig. 7. Relative population of molecules in triplet states $A\ ^3\Sigma_u^+$ (A,□), $B\ ^3\Pi_g$ (B,○), and $C\ ^3\Pi_u$ (C), for a DC discharge with $R = 0.75$ cm and $I = 20$ mA (—, experimental data) and $I = 80$ mA ($\cdots$). The measurements were taken from [97,98] (see text).
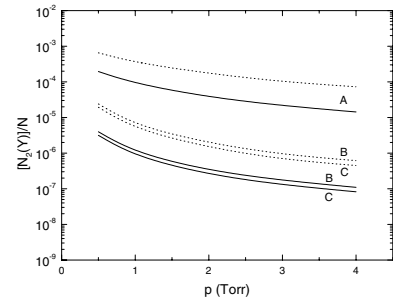

Fig. 8. Relative population of molecules in singlet states $a'\ ^1\Sigma_u^-$ (A), $a\ ^1\Pi_g$ (B), and $w\ ^1\Delta_u$ (C), with the same notation as in Figures 4–6.
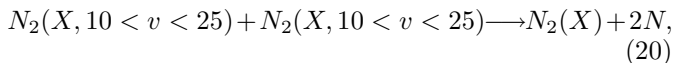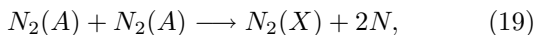
In order to compare them with the calculations and the experiments performed with $R = 0.75$ cm from [66] we have scaled the abscissas according to the similarity parameter pR (this means, for example, that a measurement at $p = 1$ torr from [97] was plotted at $p = 1/0.75 \simeq 1.33$ torr in Fig. 7). The remarkable agreement with experiment confirms the correctness of the present calculations.

The singlet intrasystem involves the states $a'\ ^1\Sigma_u^-$, $a\ ^1\Pi_g$, $w\ ^1\Delta_u$, and $a''\ ^1\Sigma_g^+$. The former three states are strongly coupled, mainly due to reactions C15 and C20. The state $N_2(a''\ ^1\Sigma_g^+)$ always presents a very small concentration, since it is strongly quenched by N_2 molecules (reaction C21). To our knowledge there is no evidence of reactions between singlets involving vibrationally excited ground-state molecules, similar to (16), but of course the possibility of this kind of reactions cannot be simply ruled out. Figure 8 shows the relative population of the singlet states, calculated for the same conditions of Figures 4–7. For the present conditions, the relative population $[N_2(a''\ ^1\Sigma_g^+)]/N$ is always less than 5×10^{-8}. Figures 7 and 8 show that the lowest metastable states, $N_2(A\ ^3\Sigma_u^+)$ and $N_2(a'\ ^1\Sigma_u^-)$ have relatively high concentrations in DC discharges, so that they can be involved in important mechanisms, such as dissociation, ionization and gas heating.
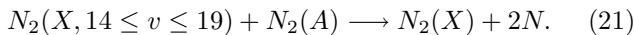
2.3.2 Dissociation

It is may be surprising that a very fundamental mechanism, as it is dissociation, is not yet completely understood in nitrogen gas discharges. What is known for a long time is that electron impact dissociation alone cannot explain the relatively high dissociation degrees observed experimentally in nitrogen discharges at pressures of about 1 torr and for values of E/N below 8×10^{-16} V.cm^2 [109]. The first suggestion to solve this question was that dissociation could take place in a purely vibration-dissociation (V-D) mechanism (cf. Tab. 3), as a result of V-V and V-T energy exchanges into a pseudo-level in the continuum [110,111]. However, the VDFs considered in those studies were unrealistically overpopulated in the high vibrational levels, since they did not take into account the deactivation of the vibrational levels at the wall [112] nor the strong V-T energy exchanges associated with N_2-N collisions [86,88] (see also Sect. 2.2). That being so, in our discharge conditions the high levels of the VDF are in general not enough populated to allow vibrational dissociation to be effective [48,89] (cf. Fig. 3 and its discussion). Therefore, additional dissociation must occur through a different mechanism. Both V-T N_2-N and wall vibrational deactivation processes were considered in [48], but the kinetics of the metastable states $N(^2D,^2P)$ was described there in a simplified and empiric way. Nevertheless, that work has shown that reaction (17) does not constitute an effective depopulation mechanism of ground-state $N(^4S)$ atoms, since most of the metastable $N(^2P)$ so created are reconverted back to $N(^4S)$. The kinetics of metastable atoms was included in [100], confirming that about 90% of the created $N(^2D)$ and $N(^2P)$ atoms give back $N(^4S)$. Finally, the problem of nitrogen dissociation was recently addressed in [49].

The need for an extra source of dissociation in nitrogen discharges was recently pointed out in [66,91,104], which have proposed, respectively, dissociation to occur through reactions

$$N_2(A) + N_2(A) \longrightarrow N_2(X) + 2N, \qquad (19)$$

$$N_2(X, 10 < v < 25) + N_2(X, 10 < v < 25) \longrightarrow N_2(X) + 2N, \qquad (20)$$

and

$$N_2(X, 14 \leq v \leq 19) + N_2(A) \longrightarrow N_2(X) + 2N. \qquad (21)$$

The first of these processes was abandoned soon later due to difficulties in the explanation of experimental data, but the necessity of another ionization channel besides direct electron impact and vibrational dissociation was clearly stressed in [104]. The remaining two mechanisms are the entries C5 and C29 from Table 5. Notice that reaction (21) is likely to take place through the excitation of the pre-dissociative levels $N_2(B\ ^3\Pi_g, v' \geq 13)$, $N_2(X, 14 \leq v \leq 19) + N_2(A) \rightarrow N_2(X) + N_2(B, v' \geq 13) \rightarrow N_2(X) + 2N$, as it is suggested in [95]. This process is very similar to the very important reaction (16), which is accepted to have a rather large rate coefficient [48,52]. An
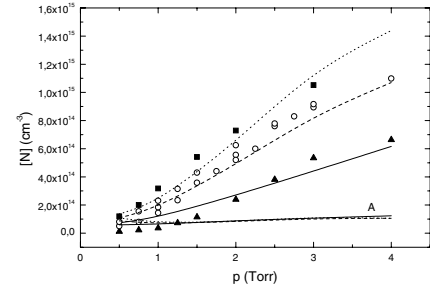

Fig. 9. Measured (points) and calculated (curves) concentrations of ground-state $N(^4S)$ atoms, for a DC discharge with $R = 0.75$ cm and $I = 20$ mA ($\blacktriangle$, —), 50 mA ($\circ$, − −) and 80 mA ($\blacksquare$, $\cdots$). Curves A are the calculation results when processes (20) and (21) are not considered.
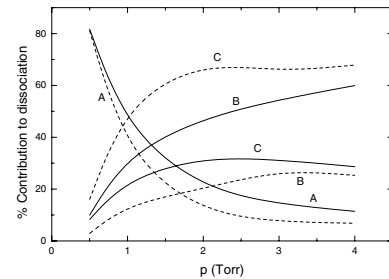

Fig. 10. Relative contribution of the different dissociation channels to the total dissociation rate, for a DC discharge with $R = 0.75$ cm and $I = 20$ mA (—) and $I = 80$ mA (− −): (A) e+$N_2 \rightarrow$ e+N+N; (B) $N_2(X,v)+N_2(X,v) \rightarrow N_2$+N+N, mechanism (20); (C) $N_2(X,v)+N_2(A) \rightarrow N_2$+N+N, process (21).

important contribution to the total dissociation rate resulting from the excitation of levels $v' \geq 13$ was also referred in [113]. It is still worth to note that at $v \geq 20$ reaction (21) does not create $N_2(B,v')$ anymore, but instead the non-dissociative state $N_2(C\ ^3\Pi_u,v')$ [95].

Figure 9 shows the comparison between calculated and measured concentrations of nitrogen $N(^4S)$ atoms in a DC discharge for the same conditions as in Figures 4–8. The electron spin resonance (ESR) experimental measurements were taken from [66]. The different sets of data are for discharge currents $I = 20$ mA (full curves and black triangles), 50 mA (dashed curves and open circles) and 80 mA (dotted curves and black squares). Curves A are the results of the calculations obtained by neglecting processes (20) and (21), i.e., considering only dissociation by direct electron impact *and* vibrational dissociation. They strikingly show the need of invoking other dissociation channels. The overall agreement between the model predictions and the measurements is quite remarkable.

In order to clarify the importance of the proposed dissociation mechanisms (20) and (21), Figure 10 depicts the relative contribution of the various dissociation processes to the total dissociation rate, for $I = 20$ mA (full curves) and $I = 80$ mA (dashed curves). The different labels correspond to the contributions of electron impact dissociation (A), dissociation according to reactions (20) (B) and (21) (C). This figure confirms that electron impact dissociation is the major dissociation channel only at

pressures below ~ 1 torr. For higher values of pressure, reactions (20) and (21) start to be effective, their contribution to dissociation reaching values as high as 90%. We can also see that reaction (20) explains the results at low values of I, whereas (21) is responsible for the good description at higher currents. Notice that Figure 10 shows the contributions to the total dissociation rate and not the contributions to the formation of N(^4S) atoms. In absolute values, N(^4S) atoms are destroyed essentially by collisions with N$_2$($A\ ^3\Sigma_u^+$) (17), and created by (18) and in the various mechanisms of quenching of N(^2D) and N(^2P) atoms listed in Table 5, in particular C26, C27, C32–C34 and C37. Nevertheless, similarly to what happens with N$_2$($A\ ^3\Sigma_u^+$) and N$_2$($B\ ^3\Pi_g$), these processes essentially redistribute the total atomic population among N(^4S), N(^2D) and N(^2P) atoms, their absolute value being basically determined by other slower processes, namely the dissociation mechanisms shown in Figure 10 and recombination at the wall. A detailed discussion of the this effect and the quantification of the importance of the different mechanisms in the creation and destruction of N(^4S) atoms can be found in [100]. Let us still note that dissociative recombination C49 can contribute significantly to dissociation in N$_2$-Ar mixtures predominantly composed by Ar [114,115], but it is totally negligible for the present conditions.

The different behavior of dissociation according to (20) and (21) cannot be attributed to any differences in E/N (see below), but rather to differences in the vibrational temperature T_V of ground-state nitrogen molecules. As it has been discussed in [49], if the ionization degree is high enough to ensure a relatively important value for T_V, the increased formation of N$_2$($A\ ^3\Sigma_u^+$) molecules (due to the changes in the EEDF caused by superelastic collisions) makes dissociation through reaction (21) a major source of N(^4S) atoms. However, this process cannot explain the experimental results at low discharge currents, where dissociation is well described by reaction (20). This mechanism may in fact correspond to an effective way of writing a sequence of other elementary processes. One possibility is the two-step process $2N_2(X, v > 16) \rightarrow N_2(X) + N_2(a')$ followed by $N_2(X, v \geq 7) + N_2(a') \rightarrow N_2(a, v' \geq 6) \rightarrow N_2(X) + N + N$. The first of these reactions is considered in [71], while the second one is similar to (21). The direct excitation of N$_2$($B\ ^3\Pi_g, v'$) and N$_2$($a\ ^1\Pi_g, v''$) in the pre-dissociative levels $v' \geq 13$ and $v'' \geq 6$ is also possible. For example, reaction $2N_2(X, v > 13) \rightarrow N_2(X) + N_2(B)$ is reported in [71,95]. Finally, it is still possible for vibrational dissociation to play some role at low discharge currents, in case we are considering too strong V-T rates N$_2$-N (see Sects. 2.2 and 3). But even in this situation it cannot possibly replace (21) and explain the results at higher ionization degrees.

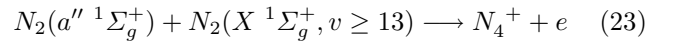### 2.3.3 Ionization and charged particles

The problem of ionization in nitrogen discharges has some similarities with the question of dissociation just described. As a matter of fact, it is well established that direct electron impact ionization alone cannot justify the ionization rate experimentally observed for pressures above ~ 1 torr [116]. That being so, other important ionization paths must exist. The difficulty of accurate calculations of ionization at low E/N was also emphasized and addressed in [117].

Two different tendencies appeared in the literature suggesting additional ionization channels. The first one attempts to explain the experimental data invoking processes that involve vibrationally excited ground state molecules [116,118,119]. In particular, reactions
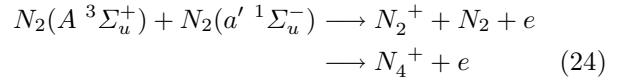
$$N_2(X\ ^1\Sigma_g^+, v \geq 32) + N_2(X\ ^1\Sigma_g^+, v \geq 32) \longrightarrow N_4^+ + e \tag{22}$$

and

$$N_2(a''\ ^1\Sigma_g^+) + N_2(X\ ^1\Sigma_g^+, v \geq 13) \longrightarrow N_4^+ + e \tag{23}$$
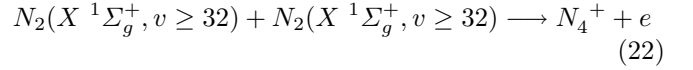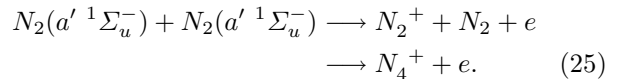
were proposed. However, the same comments made about vibrational dissociation can be repeated here: the VDF of ground-state nitrogen molecules is generally not strong enough populated in the high vibrational levels to allow reactions (22) to be efficient. Furthermore, the metastable state N$_2$($a''\ ^1\Sigma_g^+$) is strongly quenched by N$_2$ (reaction C21) [62]. As it was already referred, the relative population of this state is always less than 10^{-8}, so that process (23) cannot contribute significantly to ionization. Notice as well that reaction (22) was retracted [119], where it has been suggested it could somehow be an effective representation of a sequence of other elementary steps.

The second trend emphasizes ionization as a result of collisions between metastable electronic states [120–122], according to reactions C41 and C42 from Table 5,

$$N_2(A\ ^3\Sigma_u^+) + N_2(a'\ ^1\Sigma_u^-) \longrightarrow N_2^+ + N_2 + e$$
$$\longrightarrow N_4^+ + e \tag{24}$$

and

$$N_2(a'\ ^1\Sigma_u^-) + N_2(a'\ ^1\Sigma_u^-) \longrightarrow N_2^+ + N_2 + e$$
$$\longrightarrow N_4^+ + e. \tag{25}$$

The problem of ionization in nitrogen discharges was analyzed in [48], where revised rate coefficients for the Penning/associative ionization reactions (24) and (25) were proposed. Another argument in favor of this second trend was given in [123], in a study of the development of a discharge in the absence of electric fields, where direct ionization of molecules by electrons cannot be manifested, and for very low vibrational excitation.

To evaluate the importance of Penning/associative ionization in nitrogen discharges, Figure 11 shows the relative contribution of the different ionization channels to the total ionization rate, for the same conditions as in Figures 4–10. For the conditions here under study, Penning/associative ionization is by far the dominant ionization channel, through reactions (24) and (25). On the contrary, the contribution of stepwise ionization (processes C43–C47, the most important being C44) is usually negligible and always less than 8%.
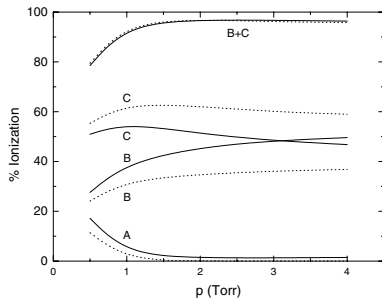
Fig. 11. Relative contribution of the different ionization channels to the total ionization rate, for a DC discharge with $R = 0.75$ cm and $I = 20$ mA (—) and $I = 80$ mA (– –): (A) e+N$_2$ → e+e+N$_2^+$; (B) N$_2(A)$+N$_2(a')$ → N$_4^+$+e, mechanism (24); (C) N$_2(a')$+N$_2(a')$ → N$_4^+$+e, process (25).

The significance of Penning/associative ionization was beautifully demonstrated from the measurements of E/N in N$_2$-O$_2$ [124] and N$_2$-H$_2$ [104] DC discharges. E/N was found to increase when O$_2$ and H$_2$ is added to a nitrogen discharge. This effect was explained as a consequence of the destruction of N$_2(A\ ^3\Sigma_u^+)$ and N$_2(a'\ ^1\Sigma_u^-)$ metastable states in collisions with O$_2$, O, H$_2$ and H, which leads to a reduction of the net rate of Penning/associative ionization so that the reduced electric field must increase to sustain the discharge [124,125].

The concentrations of the different charged particles can be calculated from their respective continuity equations. Besides direct electron impact ionization, we have taken into account mechanisms C41–C53 from Table 5. Notice that it is quite irrelevant to consider reactions (24) and (25) as Penning or associative ionization processes (i.e., producing N$_2^+$+N$_2$+e or N$_4^+$+e, respectively), since the populations of N$_2^+$ and N$_4^+$ ions are quickly redistributed by C51 and C52. In the present calculations we have rather arbitrarily taken a branching ration of 0.5 for each of the two possible products of ionization via (24) and (25). In the presence of n species of positive ions, the ambipolar diffusion coefficient for a certain species i, $D_{a,i}$, is given by

$$D_{a,i} = D_i - \mu_i \frac{\sum_{j=1}^{n+1} n_j D_j}{\sum_{j=1}^{n+1} n_j \mu_j} \quad i = 1, \ldots, n+1, \quad (26)$$

where the index $n+1$ corresponds to electrons, D_i and μ_i are the free diffusion coefficient and the mobility for species i, respectively, the later taken as positive for the ions and negative for the electrons, and n_i is the concentration of the ionic species i, with $n_{n+1} = -n_e$, n_e denoting the electron density. When the ion temperature, T_i, is much lower than the electron temperature, T_e, this expression gives approximately

$$D_{a,i} \simeq D_i \frac{T_i}{T_e} \quad i = 1, \ldots, n, \quad (27)$$

for the positive ion i, and

$$D_{a,e} \simeq \sum_i^n \frac{n_i}{n_e} D_{a,i} = \sum_i^n \frac{n_i}{n_e} D_i \frac{T_i}{T_e} \quad (28)$$
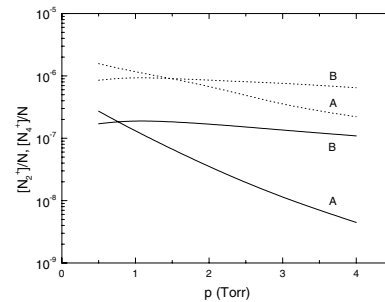

Fig. 12. Relative population of N$_2^+$ (A) and N$_4^+$ (B), for a DC discharge with $R = 0.75$ cm and $I = 20$ mA (—) and $I = 80$ mA (– –).

for the electrons. Notice that we must always have $n_e D_{a,e} = \sum_{i=1}^n n_i D_{a,i}$. Figure 12 exhibits the calculated relative concentrations of N$_2^+$ and N$_4^+$ ions are for the same conditions as in the previous figures, confirming that above $\sim$1 torr N$_4^+$ is the primary ion.

2.3.4 Gas heating

It is of course abusive to consider gas heating as part of the "chemical kinetics". Nevertheless, if the electron, vibrational and chemical kinetics have been studied, it takes just a small step to investigate the gas heating in nitrogen discharges and we think it is worth to do it. The analysis of gas heating in nitrogen and nitrogen-argon surface-wave discharges was performed in [89,107,114,115].

Neglecting axial transport and assuming a parabolic radial profile for the gas temperature, the stationary gas thermal balance equation takes the well known form

$$\frac{8\lambda(T_g)}{R^2}(T_g - T_w) = Q_{in}, \quad (29)$$

where T_w denotes the wall temperature, Q_{in} is the mean input power transferred to the translational mode per volume unit, λ is the thermal conductivity, taken from [126], and T_g is the radially averaged gas temperature. The gas temperature in the axis in this case is equal to $2T_g - T_w$.

The calculations of the total gas heating (r.h.s. term of the gas thermal balance equation) take into account all collision processes that lead to the transfer of energy to the translation mode. For the a discharge in pure nitrogen, the different gas heating channels are as follows:

(i) vibration-vibration (V-V) energy exchange processes in N$_2$-N$_2$ collisions, i.e., non-resonant reactions of the form (cf. Tab. 3)

$$N_2(X,v) + N_2(X,w-1) \xrightarrow{Q_{v,v-1}^{w-1,w}}$$
$$N_2(X,v-1) + N_2(X,w), \quad (30)$$
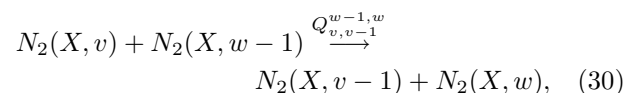
to which correspond a mean input power to the translation mode given by

$$Q_{in}^{V-V} = \sum_{v=1}^{45} [N_2(X,v)]$$
$$\times \sum_{w=1}^{45} [N_2(X,w-1)] Q_{v,v-1}^{w-1,w} \Delta E_{v,v-1}^{w-1,w}, \quad (31)$$

where $[M]$ is the volume density of species M, $Q_{v,v-1}^{w-1,w}$ is the rate coefficient for this process, $\Delta E_{v,v-1}^{w-1,w} = 2\hbar\omega\chi_e(w-v)$ is the energy available from this reaction, and $\omega = 4.443 \times 10^{14}$ s^{-1} and $\chi_e = 6.073 \times 10^{-3}$ are the spectroscopic constants for the anharmonic Morse oscillator describing the energies of the vibrational levels, $E_v = \hbar\omega\left[(v+1/2) - \chi_e(v+1/2)^2\right]$ [55];

(ii) vibration-translation (V-T) energy exchange processes in N$_2$-N$_2$ collisions,

$$N_2(X,v) + N_2 \xrightarrow{P_{v,v-1}} N_2(X,v-1) + N_2, \quad (32)$$
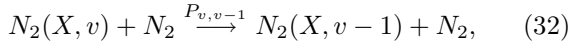
with

$$Q_{in}^{V-T} = [N_2] \sum_{v=1}^{45} \left([N_2(X,v)] P_{v,v-1}\right.$$
$$\left. - [N_2(X,v-1)] P_{v-1,v}\right) \Delta E_{v,v-1}, \quad (33)$$

where $\Delta E_{v,v-1} = \hbar\omega(1-2\chi_e v)$;

(iii) vibration-translation (V-T) energy exchange processes in multi-quantum N$_2$-N collisions,

$$N_2(X,v) + N \xrightarrow{P_{v,w}^{N_2-N}} N_2(X,w<v) + N, \quad (34)$$
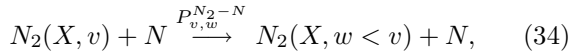
with

$$Q_{in}^{N_2-N} = [N] \sum_{v=1}^{45} [N_2(X,v)] \sum_{w=0}^{v-1} P_{v,w}^{N_2-N} \Delta E_{v,w},$$
$$(35)$$

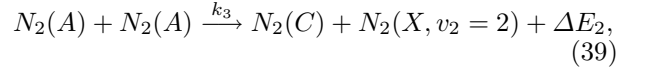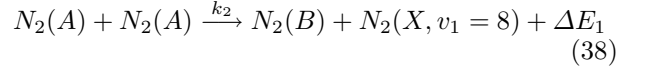where $\Delta E_{v,w} = \hbar\omega(v-w)\left[1 - \chi_e(v+w+1)\right]$;

(iv) electron elastic and rotational losses, which are obtained from the appropriate integrals on the calculated EEDF,

$$Q_{in}^{el} = n_e[N_2] \int_0^\infty G_c \, du \quad (36)$$

$$Q_{in}^{rot} = n_e[N_2] \int_0^\infty G_{rot} \, du, \quad (37)$$

where G_c and G_{rot} are the energy fluxes driven by electron elastic collisions and excitation and de-excitation of rotational levels, defined in equations (4) and (6);

(v) exothermic pooling reactions of N$_2(A\ ^3\Sigma_u^+)$ (reactions C2 and C3 in Tab. 5),

$$N_2(A) + N_2(A) \xrightarrow{k_2} N_2(B) + N_2(X,v_1=8) + \Delta E_1$$
$$(38)$$

$$N_2(A) + N_2(A) \xrightarrow{k_3} N_2(C) + N_2(X,v_2=2) + \Delta E_2,$$
$$(39)$$

with $\Delta E_1 = 2$ eV and $\Delta E_2 = 0.4$ eV and

$$Q_{in}^{N_2(A)} = [N_2(A)]^2 (k_2\Delta E_1 + k_3\Delta E_2); \quad (40)$$

(vi) vibrational deactivation at the wall (see Tab. 3), with

$$Q_{in}^{Wall} = \sum_{v=1}^{45} [N_2(X,v)]\nu_w \Delta E_{v,v-1}\beta; \quad (41)$$

(vii) deactivation of electronic metastable states at the wall (see Tab. 5), with

$$Q_{in}^Y = [M(Y)]\frac{D_Y}{\Lambda^2}\Delta E_Y\beta, \quad (42)$$

where we consider the species $M(Y) = N_2(A\ ^3\Sigma_u^+)$, N$_2(a'\ ^1\Sigma_u^-)$, N($^2D$) and N($^2P$), ΔE_Y is the energy of the corresponding excited state and D_Y its diffusion coefficient.

In these expressions, β is the accommodation coefficient, determining the part of the available energy in the deactivation electronically or vibrationally excited metastable species at the wall that is absorbed by it, being the remaining energy returned to the gas phase. For lack of data we have simply taken $\beta = 0.5$. The effect of considering other values for the accommodation coefficient were discussed in [89]. The neutralization of ions at the wall with generation of hot neutrals, which is very important in argon [127], starts to be noticeable only below ∼1 torr and for the higher discharge currents. For the present conditions its contribution is always less than 7%.

The pooling reactions of N$_2(A\ ^3\Sigma_u^+)$ metastables, corresponding to equations (38) and (39), are known to play a role in the gas heating at the first instants of the discharge, before a stationary situation is reached [46,128]. They can be important in discharge conditions as well, if the metastable state N$_2(A\ ^3\Sigma_u^+)$ is efficiently populated [89]. Notice that we have assumed that half of the energy available in the pooling reactions goes to the translational mode, while the other is transformed into vibrational energy, in accordance with [46,129,130]. This assumption, that leads to $v_1 = 8$ and $\Delta E_1 = 2.0$ eV in equation (38), and to $v_2 = 2$ and $\Delta E_2 = 0.4$ eV in equation (39), nearly corresponds to an energy balance model with the reactions obeying to the Franck-Condon principle [46].

Figures 13 and 14 describe, respectively, the gas temperature and the relative contribution of the different heating channels to the gas heating for a DC discharge with $R = 0.75$ cm and $I = 20$ mA (—) and
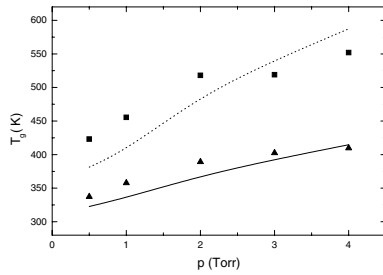
Fig. 13. Calculated (curves) and measured (points) gas temperatures for a DC discharge with $R = 0.75$ cm and $I = 20$ mA ($\blacktriangle$, —) and 80 mA ($\blacksquare$, $\cdots$).
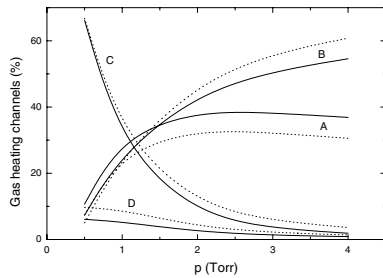

Fig. 14. Relative contribution of the different heating channels to the gas heating for a DC discharge with $R = 0.75$ cm and $I = 20$ mA (—) and 80 mA ($\cdots$): V-V processes (A); V-T N_2-N collisions (B); deactivation of metastables at the wall (C); and pooling reactions (38) and (39) (D).

$I = 80$ mA (– –). The agreement between the model predictions and the experimental measurements from [66] is quite remarkable. Figure 14 shows that the nature of gas heating changes at values of the product pR close to 1 torr.cm. At low pressures the electronically excited metastable states strongly contribute to the total gas heating, by deactivation at the wall and chemical reactions. The influence of pooling reactions is higher for $I = 80$ mA, due to the stronger population of $N_2(A\ ^3\Sigma_u^+)$ metastables in this case (see Fig. 7). For conditions of still higher electron densities, such as in a microwave surface-wave discharge, the pooling reactions can have a stronger influence than that shown here [89,107]. On the other hand, for $pR \gtrsim 1$ torr.cm vibrationally excited molecules are responsible for most of the gas heating, as a consequence of the V-V and V-T N_2-N energy relaxation mechanisms. The importance of V-V processes to the gas heating for $p = 1.5-10$ torr was pointed out in [131], even if that study neglected the effect of atoms on the V-T deactivation.

2.4 Surface kinetics

The study of the surface kinetics of atomic species, and in particular of the elementary processes leading to heterogeneous recombination, is very important in gas discharges. As a matter of fact, many of the characteristics of plasma reactors are in practice controlled by wall reactions. However, due to lack of data, surface kinetics is usually extremely simplified and surface recombination and deactivation are simply treated as effective gas-phase processes.
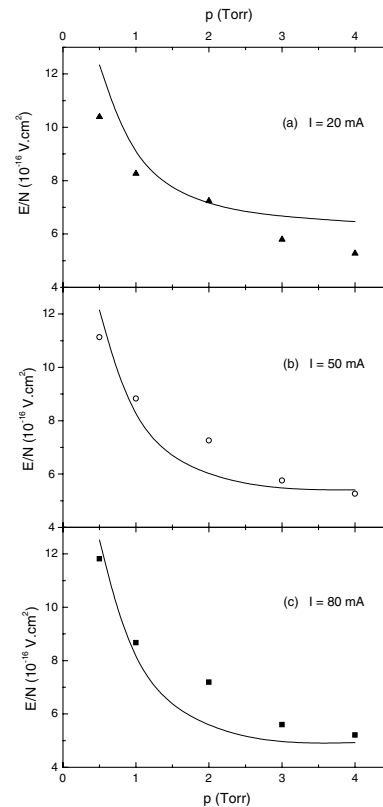

Fig. 15. Measured (points) and calculated (lines) values of the reduced electric field for a DC discharge with $R = 0.75$ and $I = 20$ mA (a), 50 mA (b) and 80 mA (c).

In this work we follow this approach. Therefore, the rate frequency of recombination is related to the recombination probability γ by
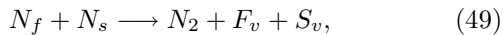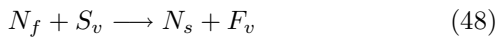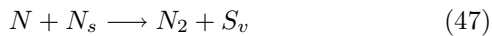
$$\nu = \frac{\gamma \langle v \rangle}{2R}, \qquad (43)$$

where $\langle v \rangle$ denotes the average velocity of the particle colliding upon the wall and R is the tube radius. Of course a similar expression is used for the wall deactivation of vibrationally excited $N_2(X\ ^1\Sigma_g^+, v)$ molecules (see Tab. 3). For constant values of γ, equation (43) reflects a first order process.

As referred in [132], one of the difficulties in the investigation of surface recombination is the inconsistency between the experimental data obtained in different experiments, which shows the great sensitivity of the results to the conditions of the surface. Thus, whenever it is possible, it is desirable to use experimental data corresponding exactly to the same conditions to be studied by modeling. For our discharge calculations we have used the value $\gamma_d = 10^{-3}$ (entry C31 in Tab. 5), obtained in [66] precisely for the conditions corresponding to the calculations shown in Figures 4–15.

There is no more to say about surface kinetics as considered in our present model. Nevertheless, we believe it is an important issue, with expected breakthroughs during the next years, so that it is worth to stress some of its aspects. Marković and co-workers have shown that

nitrogen atomic recombination may be second order in N, depending on the wall material [132,133]. This indicates that the probability of recombination, γ, is actually hiding the complex elementary processes actually occurring on the surface. The minimum sequence of elementary processes required to study nitrogen recombination in silica-based surfaces was proposed in [134], where it is assumed that the surface is totally covered with adsorption sites, which can hold atoms either reversibly (physisorption) or irreversibly (chemisorption). The list of reactions can be written as

$$N + F_v \longrightarrow N_f \tag{44}$$

$$N_f \longrightarrow N + F_v \tag{45}$$

$$N + S_v \longrightarrow N_s \tag{46}$$

$$N + N_s \longrightarrow N_2 + S_v \tag{47}$$

$$N_f + S_v \longrightarrow N_s + F_v \tag{48}$$

$$N_f + N_s \longrightarrow N_2 + F_v + S_v, \tag{49}$$

where F_v and S_v denote vacant physisorption and chemisorption sites, N_f and N_s physisorbed and chemisorbed atoms, and N and N_2 gas-phase atoms and molecules, respectively. This scheme takes into account physical adsorption and desorption of atoms at reversible sites, expressions (44) and (45); chemisorption on irreversible sites, (46); recombination of chemisorbed atoms with gas-phase atoms - Eley-Rideal (E-R) recombination, (47); surface diffusion of physisorbed atoms, (48); and recombination between a diffusing physisorbed atom and a chemisorbed one - Langmuir-Hinshelwood (L-H) recombination (49). The set of equations (44–49) can be solved in a continuous approximation, similarly to what is done for the volume chemical kinetics. Once more, one crucial point is the incorporation of physicochemical quantities, such as, for example, atoms adsorption energies, sticking coefficients, number of sites per unit area and others. There is still a large range of uncertainty in the determination of these quantities and it is common to find models with relatively complicated expressions for steric factors that are used to cover these gaps. It is still worth to note that a simple adsorption-phonon mechanism was used in [135] to study the heterogeneous relaxation of $N_2(X\ ^1\Sigma_g^+, v = 1)$ molecules and its influence on the recombination probability of N atoms. Together with (44) and (49), this model considered adsorption, deactivation and desorption of vibrationally excited molecules on the surface.

A serious effort to develop discharge models coupling surface kinetics into nitrogen discharge models was made by Gordiets and collaborators, who extended the set of reactions (44–49) to the case of N_2-O_2 [71,136] and N_2-H_2 [104,137] mixtures. These works brought undoubtedly physical insight into the surface elementary mechanisms. However, new results from [138] seem to be inconsistent with the conclusions from [104], fact that stresses the arduousness of an harmonious treatment of surface kinetics.

Any surface model must try to describe at a detailed level the mechanisms of gas-surface interaction, in particular by providing the recombination probability, γ, the relative importance of L-H and E-R recombinations, and the wall temperature effect on the recombination coefficient. This later issue is quite interesting, since in some conditions γ does not exhibit a monotonic behavior with T_w [134,139,140]. Evidently the scheme described by (44–49) can be improved, considering other mechanisms and effects. For example, nitrogen atoms are in competition for adsorption sites with N_2 molecules, which may interfere with adsorption by atoms, depending on the respective sticking probabilities and lifetimes for desorption [133]. However, a theoretical study in the framework of Molecular Dynamics shown that N_2 is slightly or not physisorbed on silica surfaces [141]. The processes of dissociative chemisorption and abstraction can also be included, as it was done, for example, for a dissociated carbon dioxide mixture in [142]. Interactions among adsorbates often play a determining role on surfaces, and the nitrogen surface coverage may affect the reaction rate constants [143]. The conventional theories defining surface processes in terms of the concentrations and properties of the different species cannot fully describe the complex kinetics on surfaces. An obvious alternative are Monte Carlo theories. For the set of reactions (44–49), a real time dynamical Monte Carlo scheme was recently presented in [144]. Another remark is the large difference in the values of the recombination probability in the discharge and in the afterglow (see C31) observed by many authors, which raises the question of creation and destruction of chemisorption sites. The possible formation of multilayers is another subject of investigation. Finally, an important aspect in gas-surface interactions is the partitioning of energy among the internal degrees of freedom of the formed molecules. In particular, it is desirable to know which fraction of energy released in an exothermic surface reaction is transferred to the substrate (the accommodation coefficient, cf. the gas heating paragraph in Sect. 2.3) and which part is transferred to vibrational and electronic excitation of N_2. For instance, the formation of $N_2(A\ ^3\Sigma_u^+)$ on the surface has been assumed in [133,145] and later on discussed in [146,147], for the interpretation of time-delay experiments. It was also suggested to occur during the expansion of a thermal plasma [148]. The answer to these last questions may be given by molecular dynamic calculations using ab initio collisional methods [149,150], which are able to describe recombination at a very fundamental level.

2.5 Self-consistent modeling

We have already described and discussed several phenomena related to electron, vibrational, chemical and surface kinetics. It is clear that each of these kinetics is strongly coupled to the others, with the central role being played by the VDF of $N_2(X\ ^1\Sigma_g^+)$ molecules. The various kinetics can be coupled efficiently with iterative procedures going back and forth the different sets of equations

while updating the several calculated physical quantities. The self-consistent determination of the electric field can be performed as well, using the requirement that under steady-state conditions the total rate of ionization must compensate exactly for the rate of electron loss (by diffusion to the wall under the effect of the space-charge field plus electron-ion recombination), together with the assumption of a quasi-neutral discharge. Notice that, due to the nature of the continuity equations for the charged particles, once the continuity equation is satisfied for electrons, the continuity equation for the sum of the ionic concentrations is satisfied as well. In this way, the quasi-neutrality condition constitutes an additional constraint to the problem, ensuring that the ionic concentrations can be decoupled.

The comparison between the measured and calculated reduced electric field E/N is represented in Figure 15, again for a DC discharge in a tube of radius $R = 0.75$ cm and for three values of the discharge current I. The experimental data was taken from [66]. Notice that E/N slightly decreases with increasing discharge current (see also the figures in [96,48]). On one hand, this is a consequence of the higher population of $N_2(A\ ^3\Sigma_u^+)$ and $N_2(a'\ ^1\Sigma_u^-)$ metastable states at higher I, and a subsequent increase in the efficiency of Penning/associative ionization; on the other hand, the vibrational temperature T_V of ground-state nitrogen molecules increases with I, which leads to an increase in the direct ionization rate coefficient (cf. Sect. 2.1 and Fig. 2).

The results presented in Figures 3–15 illustrate some particular aspects of one of the kinetics involved in nitrogen discharges. Even though, they were all obtained from our full self-consistent model and not only by a decoupled kinetic parametric study. For a DC discharge the input parameters are the tube radius R, pressure p, wall temperature T_w and discharge current I, whereas in the microwave case I is replaced by the electronic density n_e and we need additionally the wave field frequency $\omega/2\pi$. In the calculations leading to Figures 3–12 the experimental value of the gas temperature T_g was used as an input parameter as well. However, as we have already seen, T_g can be accurately calculated from the model.

3 Afterglow

In this section we examine the flowing afterglow of a surface-wave microwave discharge operating at frequency $\omega/2\pi = 433$ MHz, pressure $p = 3.3$ torr, in a Pyrex tube of inner radius $R = 1.9$ cm. The electron density at the end of the discharge/beginning of the post-discharge is estimated to be $n_e(0) = 3 \times 10^{10}$ cm^{-3} [151], a value slightly larger than the critical value for a surface-wave propagating at 433 MHz, $n_{ec} = 1.17 \times 10^{10}$ cm^{-3}, and the value of the gas temperature in the discharge is approximately 1000 K. This afterglow is very well characterized experimentally in [151–153], allowing a detailed comparison between the model predictions and the experimental measurements. For these conditions, the calculated effective field in the discharge is $E_e/N = 4.6 \times 10^{-16}$ V.cm^2 and the

vibrational temperature of ground-state molecules, T_V, is about 6200 K.
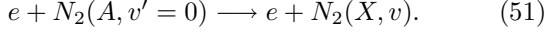
3.1 Electron kinetics

It is known that electrons are present for quite long times, as large as few ms, in the so-called short-lived afterglow [154,155]. It is therefore relevant to know the time evolution of the electron energy distribution function (EEDF) during the post-discharge. Such knowledge allows the characterization of the mechanisms involved in electron energy losses and the description of the decay of the electron mean energy and density.

The theoretical analyses of the EEDF in the nitrogen afterglow have started with the works of Capitelli and co-workers [31,129,156], devoted to the coupling between the EEDF and the vibrational distribution function (VDF) of $N_2(X\ ^1\Sigma_g^+, v)$ molecules, and in a second stage also with the kinetics of electronically excited states. Later on a Monte Carlo model was developed in [130], in which the loss of electrons was taken into account assuming a constant ambipolar diffusion coefficient. The influence of superelastic collisions with $N_2(A\ ^3\Sigma_u^+)$ metastables was investigated in [24,34], where the concentration of $N_2(A\ ^3\Sigma_u^+)$ was taken as a parameter. A coupling of the relaxation of the EEDF with the population o vibrationally excited molecules and $N_2(A\ ^3\Sigma_u^+)$ was performed in [129]. However, these three later references considered a very low degree of vibrational excitation, so that, for the present conditions, the vibrations mask the effects of superelastic collisions with $N_2(A\ ^3\Sigma_u^+)$. The effect of electron-electron collisions was studied in [24,40,157], who have shown that, in the post-discharge, electron-electron collisions significantly affect the time evolution of the EEDF for degrees of ionization as low as 10^{-6}. Winkler and co-workers have also analysed the temporal and spatial relaxation of the EEDF in different conditions, including the case of field-free relaxation [158]. A self-consistent model for the EEDF and VDF in the nitrogen afterglow was also presented in [25], where the EEDF was obtained from the solution of the steady-state Boltzmann equation. This approximation is justified if we want to look at the evolution at large times, typically bigger than $\sim 10^{-6}$–10^{-5} s, since the electron thermalization time is considerably shorter than the time variations of the populations of metastable and vibrational levels and of electrons (see below). Recently we have developed a model to study the transition from ambipolar to free diffusion regimes occurring in the afterglow [117,159] by solving the time-dependent electron Boltzmann equation including a term describing the continuous reduction of the space-charge field [157]. This model was improved in [160], in a self-consistent calculation of the temporal evolution of the EEDF and the heavy-particles, the electron Boltzmann equation comprising the term of creation of new electrons in the Penning/associative ionization reactions (24) and (25). In this article we further ameliorate the description of the electron kinetics in the afterglow with the inclusion of the excitation of $N_2(A\ ^3\Sigma_u^+, v')$ from

different vibrational levels of ground-state molecules,

$$e + N_2(X, v) \longrightarrow e + N_2(A, v'), \qquad (50)$$
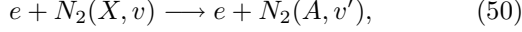
as well as superelastic collisions

$$e + N_2(A, v' = 0) \longrightarrow e + N_2(X, v). \qquad (51)$$

We recall that in [157,160] we simply considered the excitation of $N_2(A\,^3\Sigma_u^+)$ from $N_2(X\,^1\Sigma_g^+, v = 0)$. Since our kinetic scheme for heavy-particles does not discriminate the different vibrational levels of the electronically excited states (cf. Sect. 2.3), in the treatment of the superelastic collisions (51) we assume that all metastable molecules are in level $v' = 0$.

The relaxation of the EEDF in the afterglow is investigated from the solution of the time-dependent Boltzmann equation, which can be written in the form [157,160]

$$\frac{\partial F}{\partial t} + \frac{2}{3m}\frac{u}{\nu_c^e \Lambda^2}\frac{D_{se}}{D_e}F + \frac{1}{\sqrt{u}}\frac{\partial G}{\partial u} =$$
$$\frac{1}{\sqrt{u}}\sum_{i,j}\left[\sqrt{u + u_{ij}}\,\nu_{ij}(u + u_{ij})\,F(u + u_{ij}) - \sqrt{u}\,\nu_{ij}\,F\right.$$
$$\left. + \sqrt{u - u_{ij}}\,\nu_{ji}(u - u_{ij})\,F(u - u_{ij}) - \sqrt{u}\,\nu_{ji}\,F\right]$$
$$- \nu_{rec}F + \frac{1}{\sqrt{u}}\sum_{i=1}^{2}\langle\nu_{ion}^i\rangle n_e\delta(u_i). \quad (52)$$

Here, $F(u,t)$ is the EEDF in the post-discharge, but, contrary to the situation in the discharge, normalized to the electron density n_e,

$$\int_0^\infty F(u,t)\sqrt{u}\,du = n_e(t). \qquad (53)$$

Of course that $F(u, t = 0)$ is simply the EEDF calculated at the end of the discharge.

Most of the terms in equation (52) were already described in Section 2.1. $G(u)$ is the total electron flux in energy space due to the continuous terms in the Boltzmann equation, given by equations (4–6). The electric field is set to zero in the post-discharge, do that G does not include the term for the flux driven by the applied field. $\Lambda = R/2.405$ is the characteristic diffusion length for a cylindrical tube with radius R, D_{se} and D_e are the effective and free diffusion coefficients for electrons [157]. The effective diffusion coefficient is calculated from

$$D_{se} = D_a\frac{1 + \Lambda^2/\lambda_D^2}{(D_a/D_e) + \Lambda^2/\lambda_D^2}, \qquad (54)$$

with D_a and λ_D denoting the ambipolar diffusion coefficient and the Debye length.

The last two terms in equation (52) describe the electron-loss process of dissociative recombination with frequency ν_{rec} and the creation of new electrons. In the term for production of new electrons $\langle\nu_{ion}^i\rangle$, with $i = 1, 2$, represents the ionization frequency through the

Penning/associative reactions (24) and (25), respectively, defined effectively per electron as

$$\langle\nu_{ion}^1\rangle = \frac{[N_2(A)][N_2(a')]}{n_e}k_{41} \qquad (55)$$

and

$$\langle\nu_{ion}^2\rangle = \frac{[N_2(a')][N_2(a')]}{n_e}k_{42}, \qquad (56)$$

with $k_{41} = 10^{-11}$ cm^3/s and $k_{42} = 5 \times 10^{-11}$ cm^3/s (see processes C41 and C42 in Tab. 5). The new electrons are created with energies $u_1 = 0$ and $u_2 = 1.3$ eV, and the δ functions verify the usual normalization condition $\int_0^\infty \delta(u)du = 1$. As we will show, the creation of new electrons permit the description of a very interesting phenomenon, the increase of n_e in the afterglow after an initial stage of decay, as experimentally observed in [151,161].

The cross-sections for processes (50) and (51) were obtained from our basic set of cross-sections as detailed in [20], for $v = 0, \ldots, 10$ and, for the first of these reactions, $v' = 0, \ldots, 10$ as well. According to the Franck-Condon principle, the most favorable transitions for excitation/de-excitation of $N_2(A, v' = 0)$ correspond to ground-state molecules in levels $v = 5$ and $v = 6$, which have an energy threshold of 4.7 and 4.4 eV, respectively. Notice that the excitation threshold for $v' = 0$ from $v = 0$ is about 6.2 eV.

Clearly we need to know the time-dependent concentrations $[N_2(A)](t)$ and $N_2(a')](t)$ to solve the Boltzmann equation (52) in the afterglow. They are calculated from the model as it is described in Section 3.3, and subsequently introduced in (52). On the contrary, it is possible to assume a constant population of the vibrational levels $N_2(X\,^1\Sigma_g^+, v \leq 10)$ during the resolution of the Boltzmann equation, for afterglow times lower than $\sim 10^{-2}$ s (see Sect. 3.2).

Figure 16 shows the EEDF $f(u, t)$ during the afterglow, with t expressed in seconds. The EEDF is normalized to unity, $\int_0^\infty f(u)\sqrt{u}\,du = 1$, so that $F(u, t) = f(u, t)n_e(t)$. The EEDF is largely modified in the first instants of the afterglow ($t \lesssim 10^{-6}$ s), as a result of electron inelastic collisions. On the contrary, for times $t \gtrsim 10^{-6}$ s the EEDF attains a quasi-stationary state, which is due to an equilibrium achieved between the EEDF and the VDF, where the superelastic collisions of electrons with vibrationally excited molecules $N_2(X\,^1\Sigma_g^+, v)$ compensate for the inelastic vibrational losses [156,157]. The overpopulation in the region $5.5 \lesssim u \lesssim 8$ eV observed for afterglow times $10^{-6} \lesssim t \lesssim 10^{-4}$ s, in relation to the EEDFs obtained at $t = 10^{-3}$–10^{-2} s, is a direct consequence of the superelastic collisions with $N_2(A\,^3\Sigma_u^+)$ metastable molecules. This can be clearly seen in Figure 17, where we depict the EEDFs calculated for $t = 10^{-5}$ s by including (full curve) and neglecting (dotted curve) the superelastic collision process (51). The modifications in the EEDF caused by this mechanism are vanishingly small for $t \leq 10^{-7}$ s, whereas for $t \geq 10^{-3}$ s have an impact only for values of the EEDF below 10^{-5} eV$^{-3/2}$. Obviously the magnitude of the influence of process (51) depends on the population of the $N_2(A\,^3\Sigma_u^+)$ state, which is exhibited and
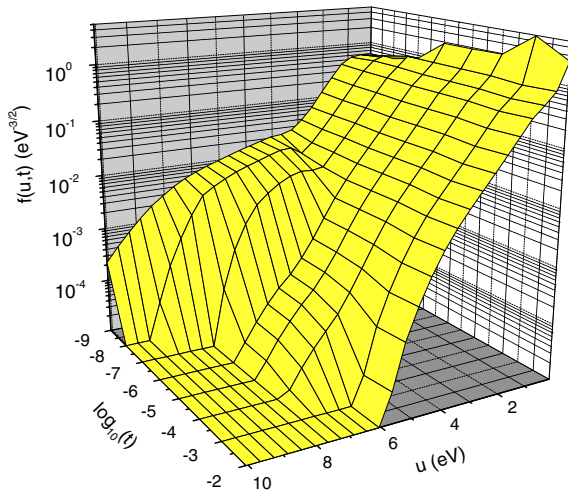
Fig. 16. Calculated EEDF in the nitrogen afterglow of a $\omega/2\pi = 433$ MHz discharge at $p = 3.3$ torr in a cylindrical tube with radius $R = 1.9$ cm, for which $E_e/N = 4.6 \times 10^{-16}$ V.cm^2 and $T_V \simeq 6200$ K. The afterglow time is expressed in seconds.
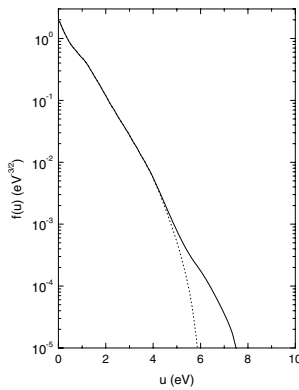

Fig. 17. Calculated EEDF in the same conditions as in Figure 16, for an afterglow time $t = 10^{-6}$ s, considering (—) and neglecting ($\cdots$) superelastic collisions with N$_2(A\ ^3\Sigma_u^+)$ molecules according to (51).

discussed in Figure 21 (Sect. 3.3). We can advance that the concentration [N$_2(A\ ^3\Sigma_u^+)$] passes through a minimum, at $t \sim 10^{-3}-10^{-2}$ s, then raising again as a consequence of the V-V up-pumping mechanism followed by V-E transfer reactions.

It is possible to see in Figure 16 the formation of a "dip" around $u \simeq 4$ eV for afterglow times in the range $10^{-8}-10^{-7}$ s (see Fig. 3 from Ref. [160] for a more evident picture). This is a result of the particular shape of the electron cross-sections for excitation of the vibrational levels N$_2(X\ ^1\Sigma_g^+, v)$, which present a strong maximum at $u \simeq 2$ eV and vanish for $u \geq 4$ eV [21,22]. The processes leading to the formation of the dip were clarified in [160]. Briefly, the behavior of electrons with energies lower than 4 eV is determined almost exclusively by the inelastic and superelastic electron-vibration (e-V) collisions. As an outcome of this mechanism, in the very beginning of the afterglow there is a loss of electrons in the 2–4 eV energy range, where the vibrational cross-section is important,

and a gain in the 0–2 eV one. On the other hand, electrons with energies between 4–6 eV do not lose appreciably their energy, since all the inelastic cross-sections are zero in this range. In other words, the frequency for loss of electrons at $u \simeq 4$ eV is higher than the frequency for loss of electrons both at $u \simeq 2-3$ eV and $u \simeq 4-6$ eV. This is the origin of the dip in the EEDF at 4 eV. It is worth to mention that a local minimum in $f(u)$, very similar in shape to the one displayed in Figure 3, was measured experimentally for a nitrogen post-discharge in [162] and for an ECR source in [163]. The dip does not get deeper and deeper as the EEDF evolves, because the frequency of loss of electrons with a certain energy u, $\nu(u)$, is not constant in time [160]. In fact, in the interval 0–4 eV the electrons lose their energy mainly in inelastic collisions with the vibrational levels, but, on the other hand, they gain energy in superelastic collisions again with the vibrational levels. Therefore, an equilibrium between the EEDF and the VDF is induced in this energy range, so that after a certain time ν is vanishingly small for $u \leq 4$ eV. When this happens the electron temperature T_e of the distribution for $0 \leq u \leq 4$ eV merely reflects the vibrational temperature. This effect was pointed out in [24,156,160] and used in [164] to derive the vibrational temperature in the afterglow from the slope of the measured EEDF in this vibrational excitation region. The low energy part of the EEDF reaches a quasi-stationary state for times as short as $t \sim 10^{-7}$ s. The calculated EEDF at $t = 6.5 \times 10^{-3}$ s compares extremely well with the measurements from [160] (see Fig. 10 from that paper), obtained for electron energies between 0 and 5 eV. This agreement is in fact a confirmation of the correctness of our discharge model in the calculation of the initial VDF. The field-free temporal decay of the EEDF was also investigated in [158], for the case of no vibrational excitation and, therefore, in the absence of e-V superelastic collisions. The calculations presented in that work hence correspond to the limit case where the dip does get deeper with time. The effect was shown in [158], where a clear analyses of the relaxation of the EEDF performed in terms of a constant dissipation frequency is made. Finally we note that the formation of the dip can only take place under certain specific conditions, related to the population of the high-energy ($u \geq 6.2$ eV) tail of the EEDF [160].

The rate coefficient for excitation of N$_2(A\ ^3\Sigma_u^+)$ along the post-discharge is represented in Figure 18. Curves A are for the total excitation rate coefficient, C_X^A, while curves B correspond to the excitation of N$_2(A\ ^3\Sigma_u^+)$ from N$_2(X\ ^1\Sigma_g^+, v = 0)$ only, $C_{X,0}^A$. As mentioned above, the former process is favored with energy thresholds of 4.7 and 4.4 eV, corresponding to the excitation from levels $v = 5$ and $v = 6$, which are strongly populated (see Sect. 3.2). These thresholds are very close the the region where the EEDF is weakly depopulated, so that C_X^A remains significant for long times in the afterglow. The full and broken curves are the calculations including and neglecting superelastic collisions (51), which slightly change the results for afterglow times between 10^{-6} and 10^{-3} s. On the contrary, in the region of the threshold for excitation from $v = 0$, around 6.2 eV, the EEDF is quickly depleted,
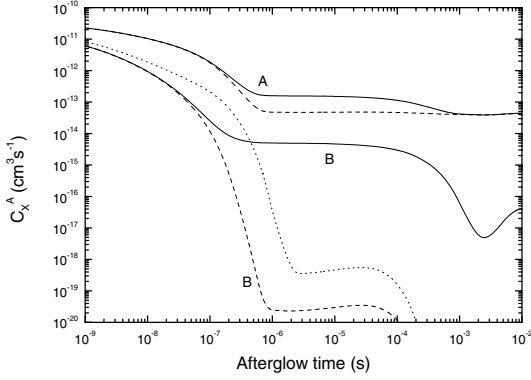
Fig. 18. Rate coefficient for excitation of state $N_2(A\ ^3\Sigma_u^+)$ as a funtion of the afterglow time, including (—) and neglecting (– –) processes (51): total rate coefficient (A); rate coefficient for the excitation from $N_2(X\ ^1\Sigma_g^+, v = 0)$ only (B). The curve (···) is the result for the conditions of [160] (see text).
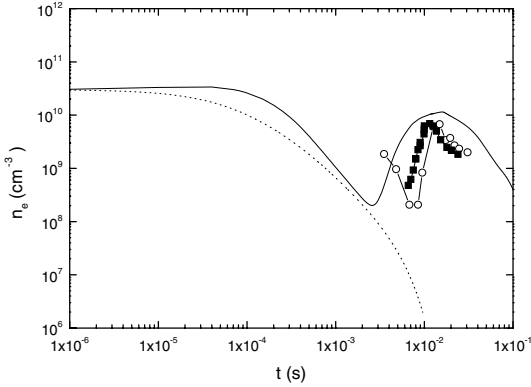

Fig. 19. Temporal evolution of the electron density in the afterglow when the creation of new electrons by reactions (24) and (25) are included (—) and neglected (···). The experimental data was taken from [151] (○) and [160] (■).

which reflects directly in rate coefficient $C_{X,0}^A$ when superelastic collisions with $N_2(A\ ^3\Sigma_u^+)$ are not taken into account (broken curve). When they are considered, $C_{X,0}^A$ starts to decrease far later, at $t \sim 10^{-4}$. However it raises again for $t \sim 10^{-3}$ s, due to the already mentioned increase in the population of $N_2(A\ ^3\Sigma_u^+)$ metastables. The dotted curve in Figure 18 is the rate coefficient obtained in the conditions of our previous investigation [160], i.e., neglecting superelastic collisions (51) and assuming the excitation of the $N_2(A\ ^3\Sigma_u^+)$ state as a single loss process at 6.2 eV. Figures 16–18 demonstrate that superelastic collisions (51) can significantly change the results in the afterglow, for excitation processes with energy thresholds in the region $u \gtrsim 5.5$ eV.

Figure 19 exhibits the electron density calculated from the time-dependent Boltzmann equation, by including (full curve) and neglecting (dotted curve) the creation of new electrons in reactions (24) and (25), together with the interferometry measurements from [151] (open circles) and the probe measurements from [160] (black squares). The experiments were performed in a flowing afterglow, so that

it is necessary to convert afterglow distances in times. This was done assuming a constant mass flow. Therefore, the afterglow time at a certain position z is given by $t(z) = [T_g(0)/v(0)] \int_0^z [1/T_g(z')]dz'$, where v is the velocity of the molecules and we use the experimental profile of the gas temperature in the afterglow, $T_g(z)$, measured in [151]. A striking aspect in Figure 19 is the no-monotonic behavior of n_e, in accordance with the observations from [151,161]. The origin of this phenomenon is detailed in Sections 3.2 and 3.3. Here let us simply note that the metastable states $N_2(A\ ^3\Sigma_u^+)$ and $N_2(a'\ ^1\Sigma_u^-)$ are formed locally in the afterglow through reactions C39 and C40 from Table 5, with the subsequent creation of electrons in the Penning/associative ionization processes (24) and (25). Slow electrons remain for a long time in the afterglow, up to $t \sim 10^{-3}$ s, even in the absence of these ionization reactions (dotted curve). Actually the frequency for electron losses by diffusion to the wall is relatively small, since the characteristic times for ambipolar diffusion are quite large, as it has been calculated in [157] and measured experimentally in the breakdown time delay experiment reported in [159] and in a pulsed RF discharge in [165]. The presence of a significant number of slow electrons for a long time makes it possible that electron stepwise excitation processes with low energy thresholds, such as the excitation of $N_2(B\ ^3\Pi_g)$ or $N_2(C\ ^3\Pi_u)$ from $N_2(A\ ^3\Sigma_u+)$, are effective under post-discharge conditions. This was firstly suggested in [166,167] and calculated theoretically in [157]. However these stepwise collisions cannot produce additional ionization in the post-discharge. As mentioned above, for $t \gtrsim 10^{-6}$ s $T_e \simeq T_V \simeq constant$ and is of the order of 0.6 eV [160]. Notice as well that a high value of T_e during the time interval $t \sim 10^{-6}$–10^{-4} s, close to 1 eV, was measured in [165] in the nitrogen afterglow of an RF pulsed discharge at $p = 0.2$ torr, the slow decay of the electron temperature confirming the importance of the equilibrium between the EEDF and the VDF.

3.2 Vibrational kinetics

The vibrational kinetics in the afterglow is investigated from the time-dependent solution to the set of equations (13) describing the population of the various vibrational levels, coupled to the similar equations for the remaining heavy-particles. The calculated densities for the steady-state discharge are the initial values of the concentrations in the beginning of the post-discharge. The experimental longitudinal temperature profile measured in [151] was used as in the model. It presents a strong temperature drop at the beginning of the post-discharge, from values of about 1000 K in the discharge to 500 K in the short-lived afterglow, tending to room temperature in the late afterglow. As we have mentioned in Section 2.2, to explain the behavior of several species in the afterglow (see next section) we felt the need to reduce our rates for V-T exchanges in N_2-N collisions by a factor of 5. The implications of considering other choices for these rate coefficients were discussed and quantified in detail in [50].
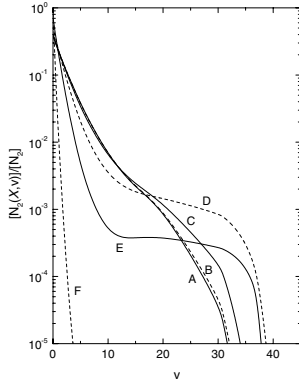
Fig. 20. VDF of $N_2(X\ ^1\Sigma_g^+)$ molecules at different instants in the afterglow: (A) $t = 0$; (B) $t = 10^{-4}$ s; (C) $t = 10^{-3}$ s; (D) $t = 10^{-2}$ s; (E) $t = 10^{-1}$ s; (F) $t = 1$ s.

The fundamental effect regarding the VDF of ground-state N_2 molecules is that the very high vibrational levels, which are not significantly populated under most discharge conditions (check Sect. 2.2), are strongly populated in the afteglow, as a result of the well known V-V up-pumping mechanism. The anharmonicity of the potential curve of $N_2(X\ ^1\Sigma_g^+)$ implies that the energy difference between neighbouring vibrational levels decreases from the bottom to the top of the vibrational ladder. Therefore, the V-V reactions from Table 3,

$$N_2(X, v) + N_2(X, w) \rightleftharpoons N_2(X, v-1) + N_2(X, w+1), \quad (57)$$
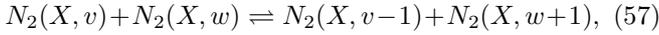
are not exactly resonant and, for $v < w$, have a larger coefficient for the forward process than for the backward one. This originates a climbing in the vibrational ladder as the e-V collisions cease to be effective [28,168]. The V-V up-pumping in the vibrational relaxation of anharmonic oscillators also exists for other diatomic molecules, such as $CO(X\ ^1\Sigma^+)$ [169,170] and $NO(X\ ^2\Pi_r)$ [171].
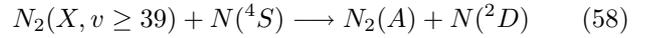
Figure 20 shows the VDFs of $N_2(X\ ^1\Sigma_g^+, v)$ molecules calculated at different afterglow times between 0 and 1 s, clearly illustrating the V-V pumping of the high v levels. The tail of the VDF passes through a maximum for afterglow times of the order of 10^{-2} s, which starts to exist for levels $v \gtrsim 25$ and is very pronounced for $v \gtrsim 35$ (see also [50,91]). This figure confirms the validity of the assumption of a near constant population in levels $0 \leq v \leq 10$ up to times $10^{-3}-10^{-2}$ s made for the solution of the time-dependent electron Boltzmann equation (52) in the previous section.
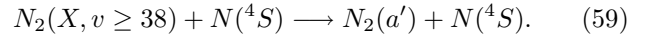
3.3 Chemical kinetics

One noteworthy feature of the nitrogen afterglow for the conditions under investigation is the presence of a dark zone at the end of the flowing discharge, before a raise of the optical emissions in the short-lived afterglow [93,152,155,172]. The enhancement of the populations detected for the radiative states $N_2(B\ ^3\Pi_g)$ and $N_2^+(B\ ^2\Sigma_u^+)$ was later confirmed to exist as well for the

metastable state $N_2(A\ ^3\Sigma_u^+)$ [151,173] and the electron density [151,160]. The presence of a dark zone indicates that metastables $N_2(A\ ^3\Sigma_u^+)$, as well as the other species mentioned above, cannot be carried out from the discharge and instead have to be created locally in the afterglow.

In a series of theoretical studies describing self-consistently both the steady-state discharge and the time-evolution in the afterglow of the electron energy distribution function and of the populations of different species, as detailed in this paper, we have shown that this behavior is a consequence of the V-V up-pumping mechanism explained in the previous Section [50,61,91]. The highly vibrationally excited dark states $N_2(X\ ^1\Sigma_g^+, v)$ formed in this way, possibly in levels as high as $v > 35$, subsequently transfer their energy to electronically excited states through V-E processes that can be mediated by heavy-particles such as N(4S) atoms (see below). The key point is the local formation of $N_2(A\ ^3\Sigma_u^+)$ and $N_2(a'\ ^1\Sigma_u^-)$ in the afterglow [50,91], which should take place in times corresponding to the pumping times for population of the highly vibrationally excited ground-state molecules. We obtained a remarkable agreement between model predictions and the available experimental measurements, by assuming that the metastable states $N_2(A\ ^3\Sigma_u^+)$ and $N_2(a'\ ^1\Sigma_u^-)$ are formed in the afterglow by collisions involving $N(^4S)$ atoms and highly vibrationally excited molecules according to reactions C39 and C40 from Table 5,
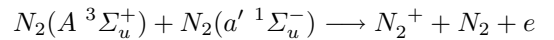
$$N_2(X, v \geq 39) + N(^4S) \longrightarrow N_2(A) + N(^2D) \quad (58)$$

and

$$N_2(X, v \geq 38) + N(^4S) \longrightarrow N_2(a') + N(^4S). \quad (59)$$
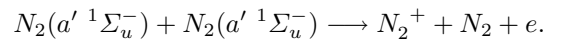
Once these two states are produced, the remaining species are readily created in a sequence of reactions described in [50,91]. $N_2(B\ ^3\Pi_g)$ is formed through reaction C4 (16),

$$N_2(A) + N_2(X, 5 \leq v \leq 14) \longrightarrow N_2(B) + N_2(X, v = 0).$$
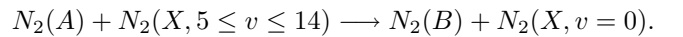
This hypothesis was confirmed in [174], where the analysis of the vibrational distribution of the $N_2(B\ ^3\Pi_g)$ state allowed to establish this process as the primary source of $N_2(B\ ^3\Pi_g)$ in N_2 post-discharges. $N_2^+(X\ ^2\Sigma_g^+)$ ions and electrons are formed by the Penning ionization mechanisms C41 (24) and C42 (25),

$$N_2(A\ ^3\Sigma_u^+) + N_2(a'\ ^1\Sigma_u^-) \longrightarrow N_2^+ + N_2 + e$$

and

$$N_2(a'\ ^1\Sigma_u^-) + N_2(a'\ ^1\Sigma_u^-) \longrightarrow N_2^+ + N_2 + e.$$

Finally the radiative species $N_2^+(B\ ^2\Sigma_u^+)$ is formed by reaction C53,

$$N_2(X, v \geq 12) + N_2^+(X) \longrightarrow N_2^+(B) + N_2(X, v - 12).$$
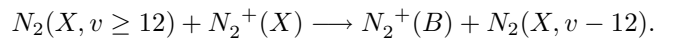
Processes (58) and (59) of resonant V-E energy transfers were experimentally observed in $CO(X\ ^1\Sigma^+, v)$ [170,175] and suggested for
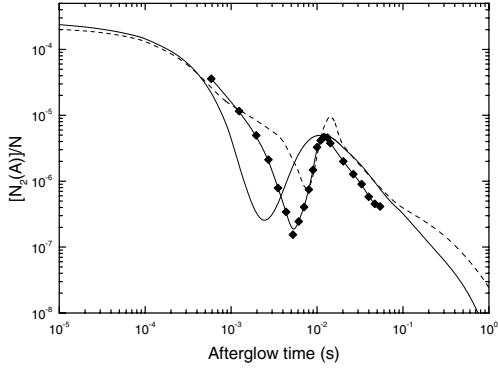
Fig. 21. Temporal evolution of the fractional concentration of $N_2(A)$ metastables in the afterglow, assuming the formation of $N_2(A)$ and $N_2(a')$ either through the mechanisms (58) and (59) (—) or through (60) and (61) (− −). The experimental data is from [151] with the correction factor of 5 pointed out in [173].
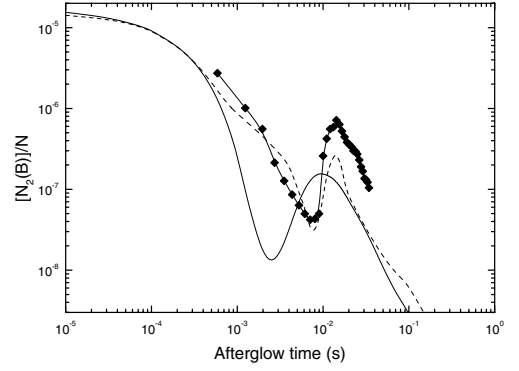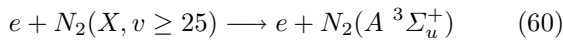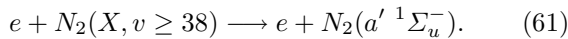

Fig. 22. Temporal evolution of the fractional concentration of $N_2(B)$ molecules in the afterglow, assuming the formation of $N_2(A)$ and $N_2(a')$ either through the mechanisms (58) and (59) (—) or through (60) and (61) (− −). The experimental data is from [179].
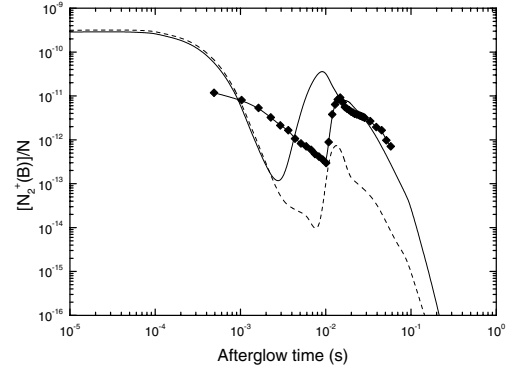

Fig. 23. Temporal evolution of the fractional concentration of $N_2^+(B)$ ions in the afterglow, assuming the formation of $N_2(A)$ and $N_2(a')$ either through the mechanisms (58) and (59) (—) or through (60) and (61) (− −). The experimental data is from [179].

$NO(X \ ^2\Pi_r, v)$ [171,176]. However, these V-E processes are far from generating consensus. For example, in [177] it is shown that for CO the inclusion of the asymmetric one-to-two quanta exchange processes allows us to explain the abrupt reduction of vibrational populations at levels $v \geq 39$ observed experimentally in [178], where it is explained by the introduction of a V-E collisional process. Nevertheless, the recent experiments reported in [170] show unambiguously that electron mediated V-E processes occur in CO, at ionization degrees as low as $10^{-9}-10^{-7}$. For this reason we suggested in [50] that resonant electron mediated vibration-electronic V-E energy transfers may contribute as well to the formation of electronically excited states in the nitrogen afterglow. The reactions of associative or Penning ionization that occur in the post-discharge can create low energy electrons able to participate nearly isoenergetic reactions. Moreover, the depopulation of high vibrational levels $N_2(X \ ^1\Sigma_g^+, v)$ by electron superelastic collisions may substantially increase the energy of these electrons.

The possible role of electron mediated V-E energy transfers can be verified by assuming, as an alternative to reactions (58) and (59), that electronically excited states can be created by reactions

$$e + N_2(X, v \geq 25) \longrightarrow e + N_2(A \ ^3\Sigma_u^+) \qquad (60)$$

and

$$e + N_2(X, v \geq 38) \longrightarrow e + N_2(a' \ ^1\Sigma_u^-). \qquad (61)$$

The rate coefficients for reactions (60) and (61) were considered to be equal to 5×10^{-9} and 5×10^{-7} cm³.s⁻¹, respectively, constant along the afterglow and independent of the vibrational level $N_2(X \ ^1\Sigma_g^+, v)$, although some particular transitions should be favored according to the Franck-Condon principle. Nevertheless, this preliminary calculation allows us to estimate the feasibility of such processes.

Figures 21–23 show the comparison between the model predictions and the experimental measurements [173,179] of the absolute concentration of $N_2(A \ ^3\Sigma_g^+)$ molecules and

the relative population of the radiative states $N_2(B \ ^3\Pi_g)$ and $N_2^+(B \ ^2\Sigma_u^+)$, respectively. We have assumed that the metastable states $N_2(A \ ^3\Sigma_u^+)$ and $N_2(a' \ ^1\Sigma_u^-)$ are created in the afterglow either from processes (58) and (59) (full curves) or from reactions (60) and (61) (dashed curves). Notice that the dashed curves do not correspond to a full self-consistent calculation, since the variation of the electron density along the post-discharge, $n_e(z)$, was taken from the experiment [151]. These figures show that the inclusion of the electron processes (60) and (61) tend to narrow the maxima for the different concentrations, allowing to obtain a good agreement with experiment for the case of $N_2(A \ ^3\Sigma_u^+)$ and $N_2(B \ ^3\Pi_g)$. The situation is different for the $N_2^+(B \ ^2\Sigma_u^+)$ state where, contrary to the results obtained considering $N(^4S)$ instead of electrons as the species colliding with $N_2(X \ ^1\Sigma_g^+, v)$, it seems difficult to justify the experimental results just with processes (60) and (61).

It is worth to mention that our calculation of the relative concentration of ground-state $N(^4S)$ atoms along the post-discharge agrees very well with the two-photon

laser-induced fluorescence measurements reported in [153] (see Fig. 3 from [91]). The fractional concentration $[\mathrm{N}(^4S)]/N$ remains unchanged and close to 10^{-2} up to $t \sim 5 \times 10^{-2}$, so that at least until this time there are always $\mathrm{N}(^4S)$ atoms available to participate in reactions (58) and (59). Therefore, the peaks in the relative concentrations of $\mathrm{N}_2(A\ ^3\Sigma_g^+)$, $\mathrm{N}_2(B\ ^3\Pi_g)$ and $\mathrm{N}_2^+(B\ ^2\Sigma_u^+)$ states, calculated assuming these two reactions, essentially reflects the behavior found for the time evolution of $\mathrm{N}_2(X\ ^1\Sigma_g^+, v \gtrsim 35)$ molecules. Note that the absolute density $[\mathrm{N}(^4S)]$ actually increases in the beginning of the afterglow due to a temperature effect, vibrational dissociation being always negligible (cf. Fig. 20).

4 Conclusions

In this paper we present a review on the kinetic modeling of low-pressure nitrogen stationary discharges and their afterglows. The complex interplay between different kinetics has been analyzed and discussed in detail. It is shown that the central role is played by the vibrationally excited $\mathrm{N}_2(X\ ^1\Sigma_g^+, v)$ molecules, which are the main energy reservoirs in nitrogen plasmas. A noticeable task is also done by electronically excited metastable states $\mathrm{N}_2(A\ ^3\Sigma_u^+)$ and $\mathrm{N}_2(a'\ ^1\Sigma_u^-)$.

The main results concerning the physics of N_2 discharges can be summarized as follows.

(i) $\mathrm{N}_2(X\ ^1\Sigma_g^+, v)$ molecules produce a significative enhancement of the high energy tail of the EEDF, as a result of e-V superelastic collisions, with the consequent increase in the rate coefficients for the various elementary processes induced by electron impact.

(ii) The excited states $\mathrm{N}_2(A\ ^3\Sigma_u^+)$ and $\mathrm{N}_2(B\ ^3\Pi_g)$ are strongly coupled, essentially in collisional intrasystem crossing,

$$N_2(B) + N_2 \longrightarrow N_2(A) + N_2$$

and

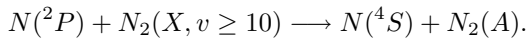$$N_2(A) + N_2(X, 5 \le v \le 14) \longrightarrow$$
$$N_2(B) + N_2(X, v = 0),$$
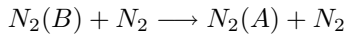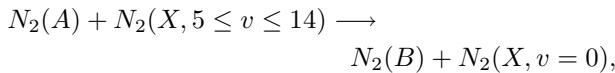
so that the combined effect of these reactions is merely a redistribution of an almost constant population among the triplet manifold. In turn, the kinetics of nitrogen atoms is interconnected with those of these two states, as a result of processes
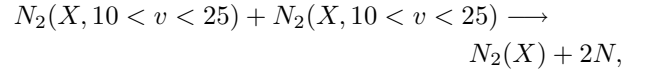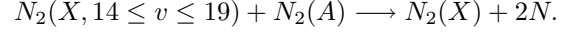
$$N_2(A) + N(^4S) \longrightarrow N_2(X, 6 \le v \le 9) + N(^2P)$$

and

$$N(^2P) + N_2(X, v \ge 10) \longrightarrow N(^4S) + N_2(A).$$
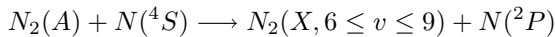
Clearly, the coupling between $\mathrm{N}_2(A\ ^3\Sigma_u^+)$, $\mathrm{N}_2(B\ ^3\Pi_g)$ and N atoms is associated with the role of vibrationally excited molecules.

(iii) At values of pR above ~ 1 torr.cm, nitrogen dissociation takes place through reactions

$$N_2(X, 10 < v < 25) + N_2(X, 10 < v < 25) \longrightarrow$$
$$N_2(X) + 2N,$$

and

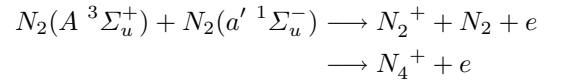$$N_2(X, 14 \le v \le 19) + N_2(A) \longrightarrow N_2(X) + 2N.$$
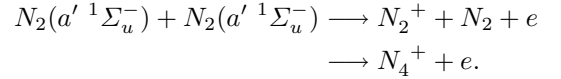
The first of these mechanisms is likely to be an effective way of writing a sequence of other elementary reactions, and it is important at low degrees of ionization. On the contrary, at high degrees of ionization the second reaction may be the major source of dissociation. Once again, the crucial role of vibrationally excited molecules is evident. However, classical vibrational dissociation very rarely can take place, due to the strong depopulation of the VDF in N_2-N collisions. The mechanisms of destruction of $\mathrm{N}(^4S)$ atoms leading to the formation of the excited states $\mathrm{N}(^2D)$ and $\mathrm{N}(^2P)$ do not constitute effective channels of destruction of ground-state atoms, since most of the excited states created in this way are de-excited back to $\mathrm{N}(^4S)$.

(iv) The metastable states $\mathrm{N}_2(A\ ^3\Sigma_g^+)$ and $\mathrm{N}_2(a'\ ^1\Sigma_g^-)$ are involved in Penning/associative processes,

$$N_2(A\ ^3\Sigma_u^+) + N_2(a'\ ^1\Sigma_u^-) \longrightarrow N_2^+ + N_2 + e$$
$$\longrightarrow N_4^+ + e$$

and

$$N_2(a'\ ^1\Sigma_u^-) + N_2(a'\ ^1\Sigma_u^-) \longrightarrow N_2^+ + N_2 + e$$
$$\longrightarrow N_4^+ + e.$$

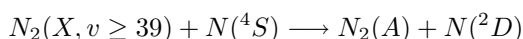For $pR \gtrsim 1$ torr.cm, the rates of these reactions largely exceeds that by electron impact.

(v) Finally, gas heating can be dominated either by V-V and V-T energy exchanges or by the electronically excited states, respectively for the higher and lower pressures.

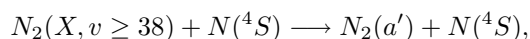Let us now go over the main points regarding N_2 post-discharges.

(i) The EEDF is quickly modified in the first instants of the afterglow, becoming a Maxwellian (with $T_e \simeq T_V$) for $u \le 4$ eV in times as short as $t \sim 10^{-7}$ s. In this energy range, the heating and cooling of electrons is due to the excitation and de-excitation processes involving vibrational levels. A full equilibrium between the EEDF and the VDF is attained at $t \sim 10^{-6}$ s, when the EEDF reaches a quasi-stationary state. However, superelastic collisions with $\mathrm{N}_2(A\ ^3\Sigma_g^+)$ metastables may have a remarkable effect on the EEDF at $u \ge 4$ eV.

(ii) Slow electrons remain for a long time in the afterglow, as a result of the large characteristic times for electron losses by ambipolar diffusion, together with the

creation of new electrons in Penning/associative reactions. This facts suggests electrons can be involved in low energy threshold processes, such as vibrational and stepwise excitation, or mediate V-E exchanges.
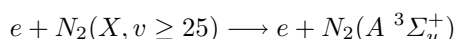
(iii) Flowing N_2 discharges are known to generate the emission bands associated with the 1^+ and 1^- systems, downstream from the discharge after a dark zone positioned at the end of the discharge. The same profile is also exhibited by the electron density. This peculiar behavior can be justified only by the creation of the electronic species $N_2(A\ ^3\Sigma_g^+)$ and $N_2(a'\ ^1\Sigma_g^-)$ locally in the afterglow. The observed peaks in the populations of the several species that occur in the afterglow are well explained by V-E mechanisms involving highly vibrationally excited N_2 molecules, that can be induced both by $N(^4S)$ atoms and by electrons. The former possibility corresponds to reactions
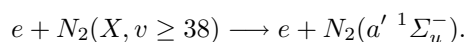
$$N_2(X, v \geq 39) + N(^4S) \longrightarrow N_2(A) + N(^2D)$$

and

$$N_2(X, v \geq 38) + N(^4S) \longrightarrow N_2(a') + N(^4S),$$

whereas the latter is described by

$$e + N_2(X, v \geq 25) \longrightarrow e + N_2(A\ ^3\Sigma_u^+)$$

and

$$e + N_2(X, v \geq 38) \longrightarrow e + N_2(a'\ ^1\Sigma_u^-).$$

In any case, the crucial effect is the V-V up-pumping mechanism, which is the climbing in the vibrational ladder resulting from near-resonant V-V energy exchanges that occurs during the relaxation process of the VDF. Thus, molecules in very high vibrational levels, whose concentrations are negligible in the discharge, become available to participate in chemical reactions after a certain time in the afterglow. Further work is needed to clarify the relative importance of the two V-E schemes proposed here.

The interpretation of nitrogen discharges and afterglows must surely rely on the available collisional data. With all the uncertainties that still exist, one of the most striking is related to V-T exchanges in N_2-N collisions. More accurate rate coefficients for these transitions are needed in order to address some of the open questions raised in this paper. An important work is still to be done related to surface kinetics, not only in the determination of the surface and surface reaction parameters, as well as to effectively provide its self-consistent coupling with the other kinetics.

References

1. W.P. Allis, in *Handbuch der Physik*, edited by S. Flügge (Springer, Berlin, 1956), Vol. 21, pp. 383–444
2. L.S. Frost, A.V. Phelps, Phys. Rev. **127**, 1621 (1962)
3. L.C. Pitchford, A.V. Phelps, Phys. Rev. A **25**, 540 (1982)
4. R.D. White, R.E. Robson, B. Schmidt, M.A. Morrison, J. Phys. D: Appl. Phys. **36**, 3125 (2003)
5. S. Yoshida, A.V. Phelps, L.C. Pitchford, Phys. Rev. A **27**, 2858 (1983)
6. D. Loffhagen, R. Winkler, J. Phys. Chem. Ref. Data **6**, 113 (1977)
7. A.G. Engelhardt, A.V. Phelps, C.G. Risk, Phys. Rev. **135**, A1566 (1964)
8. A.V. Phelps, L.C. Pitchford, Technical Report 26, JILA Information Center Report, 1985. University of Colorado, Boulder, Colorado, USA
9. I.B. Bernstein, T. Holstein, Phys. Rev. **94**, 1475 (1954)
10. L.D. Tsendin, Sov. Phys. JETP **39**, 805 (1974)
11. V.I. Kolobov, V.A. Godyak, IEEE Trans. Plasma Sci. **23**, 503 (1995)
12. E. Tatarova, F.M. Dias, C.M. Ferreira, A. Ricard, J. Appl. Phys. **85**, 49 (1999)
13. F.M. Dias, E. Tatarova, C.M. Ferreira, J. Appl. Phys. **83**, 4602 (1998)
14. C.M. Ferreira, F.M. Dias, E. Tatarova, Travelling wave discharges in nitrogen: Modelling and experiment, in *Advanced Technologies Based on Wave and Beam Generated Plasmas*, edited by H. Schluter, A. Shivarova (Kluwer Academic Publishers, 1998), pp. 311–334
15. J. Loureiro, Phys. Rev. E **47**, 1262 (1993)
16. C.M. Ferreira, J. Loureiro, J. Phys. D: Appl. Phys. **17**, 1175 (1984)
17. C.M. Ferreira, M. Moisan, Phys. Scripta **38**, 382 (1988)
18. N.L. Aleksandrov, I.V. Kochetov, A.P. Napartovich, High Temp. **23**, 666 (1986)
19. M. Cacciatore, M. Capitelli, C. Gorse, Chem. Phys. **66**, 141 (1982)
20. J. Loureiro, C.M. Ferreira, J. Phys. D: Appl. Phys. **22**, 67 (1989)
21. L.C. Pitchford, A.V. Phelps, Bull. Am. Phys. Soc. **27**, 109 (1982)
22. A.V. Phelps, Technical Report 28, JILA Information Center Report, 1985, University of Colorado, Boulder, Colorado, USA
23. J. Loureiro, C.M. Ferreira, J. Phys. D: Appl. Phys. **19**, 17 (1986)
24. N.A. Dyatko, I.V. Kochetov, A.P. Napartovich, J. Phys. D: Appl. Phys. **26**, 418 (1993)
25. N.A. Dyatko, Y.Z. Ionikh, N.B. Kolokolov, A. Meshchanov, A.P. Napartovich, IEEE Trans. Plasma Sci. **31**, 553 (2003)
26. A.A. Mihajlov, V.D. Stojanović, Z.Lj. Petrović, J. Phys. D: Appl. Phys. **32**, 2620 (1999)
27. V. Guerra, A.A. Mihajlov, Z.Lj. Petrović, J. Loureiro, Self-consistent modelling of nitrogen discharges: influence of the cross-sections for transitions between vibrational levels, in *XVIIth Europhysics Conference on Atomic and Molecular Physics of Ionized Gases (ESCAMPIG), Constanţa, Romania, 2004*, accepted
28. C.E. Treanor, J.W. Rich, R.G. Rehm, J. Chem. Phys. **48**, 1798 (1968)
29. B.F. Gordiets, S.S. Mamedov, L.A. Shelepin, Sov. Phys. - JETP **40**, 640 (1975)
30. M. Capitelli, M. Dilonardo, C. Gorse, Chem. Phys. **56**, 29 (1981)
31. C. Gorse, M. Cacciatore, M. Capitelli, S. de Benedictis, G. Dilecce, Chem. Phys. **119**, 63 (1988)

32. C.M. Ferreira, J. Loureiro, J. Phys. D: Appl. Phys. **22**, 76 (1989)

33. W.L. Nighan, Phys. Rev. A **2**, 1989 (1970)

34. F. Paniccia, C. Gorse, J. Bretagne, M. Capitelli, J. Appl. Phys. **59**, 4004 (1986)

35. F. Paniccia, C. Gorse, M. Cacciatore, M. Capitelli, J. Appl. Phys. **61**, 3123 (1987)

36. A.V. Bodronosov, K.A. Vereschchagin, O.A. Gordeev, V.V. Smirnov, V.A. Shakhatov, High Temp. **34**, 656 (1996)

37. K.A. Vereschchagin, V.V. Smirnov, V.A. Shakhatov, Tech. Phys. **67**, 487 (1997)

38. J. Loureiro, A. Ricard, J. Phys. D: Appl. Phys. **26**, 163 (1993)

39. P.A. Sá, J. Loureiro, C.M. Ferreira, J. Phys. D: Appl. Phys. **25**, 960 (1992)

40. G. Colonna, C. Gorse, M. Capitelli, R. Winkler, J. Wilhelm, Chem. Phys. Lett. **213**, 5 (1993)

41. S.D. Rockwood, Phys. Rev. A **8**, 2348 (1973)

42. N.L. Aleksandrov, A.M. Konchakov, E.E. Son, High Temp. **17**, 179 (1979)

43. V. Guerra, M.J. Pinheiro, B.F. Gordiets, J. Loureiro, C.M. Ferreira, Plasma Sources Sci. Technol. **6**, 373 (1997)

44. D. Levron, A.V. Phelps, J. Chem. Phys. **69**, 2260 (1978)

45. L.G. Piper, J. Chem. Phys. **88**, 6911 (1988)

46. J.P. Boeuf, E.E. Kunhardt, J. Appl. Phys. **60**, 915 (1986)

47. L.G. Piper, J. Chem. Phys. **88**, 231 (1988)

48. V. Guerra, J. Loureiro, Plasma Sources Sci. Technol. **6**, 361 (1997)

49. V. Guerra, E. Galiaskarov, J. Loureiro, Chem. Phys. Lett. **371**, 576 (2003)

50. P.A. Sá, V. Guerra, J. Loureiro, N. Sadeghi, J. Phys. D: Appl. Phys. **37**, 221 (2004)

51. L.G. Piper, J. Chem. Phys. **90**, 7087 (1989)

52. L.G. Piper, J. Chem. Phys. **97**, 270 (1992)

53. R.F. Heidner, D.G. Sutton, S.N. Suchard, Chem. Phys. Lett. **37**, 243 (1976)

54. L.G. Piper, J. Chem. Phys. **91**, 864 (1989)

55. A. Lofthus, P.H. Krupenie, J. Phys. Chem. Ref. Data **6**, 113 (1977)

56. L.G. Piper, J. Chem. Phys. **87**, 1625 (1987)

57. I.A. Kossyi, A.Yu. Kostinsky, A.A. Matveyev, V.P. Silakov, Plasma Sources Sci. Technol. **1**, 207 (1992)

58. W.J. Marinelli, William J. Kessler, B.D. Green, William A.M. Blumberg, J. Chem. Phys. **90**, 2167 (1989)

59. R.S. Freund, J. Chem. Phys. **56**, 4344 (1972)

60. M.E. Fraser, W.T. Rawlins, S.M. Miller, J. Chem. Phys. **88**, 538 (1988)

61. P.A. Sá, J. Loureiro, J. Phys. D: Appl. Phys. **30**, 2320 (1997)

62. A.B. Wedding, J. Borysow, A.V. Phelps, J. Chem. Phys. **98**, 6227 (1993)

63. J. Bacri, A. Medani, Physica B+C **112**, 101 (1982)

64. E.C. Zipf, R.W. McLaughlin, Planet. Space Sci. **26**, 449 (1978)

65. K.A. Berrington, P.G. Burke, W.B. Robb, J. Phys. B: At. Mol. Phys. **8**, 2500 (1975)

66. I.N. Brovikova, E.G. Galiaskarov, High Temp. **39**, 809 (2001)

67. T. Yamashita, J. Chem. Phys. **70**, 4248 (1979)

68. G. Cernogora, *Étude des États Métastables de l'Azote Atomique dans des Décharges Luminescentes*, Ph.D. thesis, Université de Paris-Sud, Orsay-France, 1980

69. T.G. Slanger, G. Black, J. Chem. Phys. **64**, 4442 (1976)

70. R.S. Freund, R.C. Wetzel, R.J. Shul, Phys. Rev. A **41**, 5861 (1990)

71. B.F. Gordiets, C.M. Ferreira, V.L. Guerra, J.M.A.H. Loureiro, J. Nahorny, D. Pagnon, M. Touzeau, M. Vialle, IEEE Trans. Plasma Sci. **23**, 750 (1995)

72. H. Böhringer, F. Arnold, J. Chem. Phys. **77**, 5534 (1982)

73. J. Anketell, Can. J. Phys. **55**, 1134 (1977)

74. J.B. Hasted, *Physics of Atomic Collisions*, 2nd edn. (Butterworths, London, 1972)

75. R.N. Schwartz, Z.I. Slawsky, K.F. Herzfeld, J. Chem. Phys. **20**, 1591 (1952)

76. R.N. Schwartz, K.F. Herzfeld, J. Chem. Phys. **22**, 767 (1954)

77. J. Keck, G. Carrier, J. Chem. Phys. **43**, 2284 (1965)

78. K.N.C. Bray, J. Phys. B: At. Mol. Phys. **1**, 705 (1968)

79. I.V. Adamovich, S.O. Macheret, J.W. Rich, C.E. Treanor, J. Thermophys. Heat Trans. **12**, 57 (1998)

80. I.V. Adamovich, AIAA J. **39**, 1916 (2001)

81. G.D. Billing, E.R. Fisher, Chem. Phys. **43**, 395 (1979)

82. O.A. Gordeev, V.A. Shakhatov, Tech. Phys. **40**, 656 (1995)

83. T. Ahn, I.V. Adamovich, W.R. Lempert, Chem. Phys. **298**, 233 (2004)

84. R.J. Frost, I.W.M. Smith, Chem. Phys. Lett. **140**, 499 (1987)

85. I. Armenise, M. Capitelli, E. Garcia, C. Gorse, A. Laganà, S. Longo, Chem. Phys. Lett. **200**, 597 (1992)

86. V. Guerra, J. Loureiro, J. Phys. D: Appl. Phys. **28**, 1903 (1995)

87. A. Laganà, G. Ochoa de Aspuru, E. Garcia, Quasiclassical and quantum rate coefficients for the N+N$_2$ reaction, Technical report, Università degli Studi di Perugia, 1996

88. E. Garcia, A. Laganà, J. Phys. Chem. **101**, 4734 (1997)

89. V. Guerra, E. Tatarova, F.M. Dias, C.M. Ferreira, J. Appl. Phys. **91**, 2648 (2002)

90. F. Esposito, M. Capitelli, C. Gorse. Chem. Phys. Lett. **257**, 193 (2000)

91. V. Guerra, P.A. Sá, J. Loureiro, Plasma Sources Sci. Technol. **12**, S8 (2003)

92. G. Black, R.L. Sharpless, T.G. Slanger, J. Chem. Phys. **58**, 4792 (1973)

93. P. Supiot, D. Blois, S.D. Benedictis, G. Dilecce, M. Barj, A. Chapput, O. Dessaux, P. Goudmand, J. Phys. D: Appl. Phys. **32**, 1887 (1999)

94. P. Macko, G. Cunge, N. Sadeghi, J. Phys. D: Appl. Phys. **34**, 1807 (2001)

95. D.I. Slovetskii, *Mechanisms of Chemical Reactions in Nonequilibrium Plasmas* (Nauka, 1980)

96. G. Cernogora, L. Houchard, M. Touzeau, C.M. Ferreira, J. Phys. B: At. Mol. Phys. **14**, 2977 (1981)

97. G. Cernogora, C.M. Ferreira, L. Houchard, M. Touzeau, J. Loureiro, J. Phys. B: At. Mol. Phys. **17**, 4429 (1984)

98. C.M. Ferreira, M. Touzeau, L. Houchard, G. Cernogora, J. Phys. B: At. Mol. Phys. **17**, 4439 (1984)

99. R. Nagpal, P.K. Ghosh, J. Phys. D: Appl. Phys. **23**, 1663 (1990)

100. V. Guerra, E. Tatarova, C.M. Ferreira, Vacuum **69**, 171 (2003)

101. S.V. Pancheshnyi, S.M. Starikovskaia, A.Yu. Starikovskii, Chem. Phys. **262**, 349 (2000)

102. S.C. Haydon, M.P. Fewell, A.D. Ernest, M.J. Baldwin, Chem. Phys. **206**, 245 (1996)

103. M.P. Fewell, S.C. Haydon, A.D. Ernest, Chem. Phys. **206**, 257 (1996)
104. B.F. Gordiets, C.M. Ferreira, M.J. Pinheiro, A. Ricard, Plasma Sources Sci. Technol. **7**, 363 (1998)
105. E. Augustyniak, J. Borysow, J. Phys. D: Appl. Phys. **28**, 55 (1995)
106. R. Bachmann, X. Li, Ch. Ottinger, A.F. Vilesov, V. Wulfmeyer, J. Chem. Phys. **98**, 8606 (1993)
107. V. Guerra, P.A. Sá, J. Loureiro, J. Phys. D: Appl. Phys. **34**, 1745 (2001)
108. H. Umemoto, M. Oku, T. Iwai, J. Chem. Phys. **118**, 10006 (2003)
109. L.S. Polak, Pure Appl. Chem. **39**, 307 (1974)
110. L.S. Polak, P.A. Sergeev, D.I. Slovetskii, R.D. Todesaite, in *12th International Conference on Phenomena in Ionized Gases (ICPIG), Eindhoven, The Netherlands, 1975*, p. 65
111. M. Capitelli, M. Dilonardo, Chem. Phys. **24**, 417 (1977)
112. J. Loureiro, Chem. Phys. **157**, 157 (1991)
113. Yu.A. Mankelevich, A.F. Pal', N.A. Popov, T.V. Rakhimova, A.V. Filippov, Effect of small O_2 impurity on current dynamics of non-self-sustained discharge in N_2, edited by A. Bouchoule, J.M. Pouvesle, A.L. Thomann, J.M. Bauchire, E. Robert, *15th International Symposium on Plasma Chemistry (ISPC), Orléans, France, 2001*, Vol. IV, pp. 1521–1527
114. J. Henriques, E. Tatarova, V. Guerra, C.M. Ferreira, J. Appl. Phys. **91**, 5622 (2002)
115. J. Henriques, E. Tatarova, F.M. Dias, C.M. Ferreira, J. Appl. Phys. **91**, 5632 (2002)
116. L.S. Polak, P.A. Sergeev, D.I. Slovetskii, High Temp. **15**, 13 (1977)
117. J. Borysow, A.V. Phelps, Phys. Rev. E **50**, 1399 (1994)
118. Yu.B. Golubovskii, V.M. Telezhko, High Temp. **22**, 340 (1984)
119. L.G. Bol'shakova, Yu.B. Golubovskii, V.M. Telezhko, D.G. Stoyanov, Sov. Phys. Tech. Phys. **35**, 665 (1990)
120. H. Brunet, P. Vincent, J. Rocca-Serra, J. Appl. Phys. **54**, 4951 (1983)
121. H. Brunet, J. Rocca-Serra, J. Appl. Phys. **57**, 1574 (1985)
122. A.V. Berdyshev, I.V. Kochetov, A.P. Napartovich, Sov. J. Plasma Phys. **14**, 438 (1988)
123. V.P. Silakov, Sov. J. Plasma Phys. **14**, 708 (1988)
124. J. Nahorny, C.M. Ferreira, B. Gordiets, D. Pagnon, M. Touzeau, M. Vialle, J. Phys. D: Appl. Phys. **28**, 738 (1995)
125. R. Nagpal, A. Garscadden, Chem. Phys. Lett. **231**, 211 (1994)
126. J.O. Hirschfelder, C.F. Curtiss, R.B. Bird, *Molecular Theory of Gases and Liquids* (Wiley, New York, 1964)
127. J. Henriques, E. Tatarova, F.M. Dias, C.M. Ferreira, J. Appl. Phys. **90**, 4921 (2001)
128. N.A. Bogatov, T.V. Borodachova, M.S. Gitlin, S.V. Golubev, I.N. Polushkin, S.V. Razin, in *8th European Sectional Conference on Atomic and Molecular Physics of Ionized Gases (ESCAMPIG), Greifswald, German Democratic Republic, 1986*, pp. 386–387
129. C. Gorse, M. Capitelli, J. Appl. Phys. **62**, 4072 (1987)
130. S.K. Dhali, L.H. Low, J. Appl. Phys. **64**, 2917 (1988)
131. P.A. Sergeev, D.I. Slovetsky, Chem. Phys. **75**, 231 (1983)
132. V.Lj. Marković, M.M. Pejović, Z.Lj. Petrović, Plasma Chem. Plasma P. **16**, 195 (1996)
133. V.Lj. Marković, M.M. Pejović, Z.Lj. Petrović, J. Phys. D: Appl. Phys. **27**, 979 (1994)
134. Y.C. Kim, M. Boudart, Langmuir **7**, 2999 (1991)
135. J. Levaton, J. Amorim, A. Rogério Sousa, D. Franco, A. Ricard, J. Phys. D: Appl. Phys. **35**, 689 (2002)
136. B.F. Gordiets, C.M. Ferreira, AIAA J. **36**, 1643 (1998)
137. B.F. Gordiets, C.M. Ferreira, M.J. Pinheiro, A. Ricard, Plasma Sources Sci. Technol. **7**, 379 (1998)
138. I.N. Brovikova, E.G. Galiaskarov, High Energy Chem. **37**, 341 (2003)
139. V.L. Kovalev, O.N. Suslov, G.A. Tirskiy, in *Molecular Physics and Hypersonic Flows*, edited by M. Capitelli, volume C 482 of NATO ASI Series (Kluwer, 1996), pp. 193–202
140. V. Guerra, Theoretical investigation of the dependence of the probability of atomic surface recombination with the wall temperature, in *XVIIth Europhysics Conference on Atomic and Molecular Physics of Ionized Gases (ESCAMPIG), Constanţa, Romania, 2004*, accepted
141. M. Cacciatore, M. Rutigliano, N. Peretti, N. Sanna, Nitrogen atom recombination on silica surface: Recombination probability and energy flows, edited by R. d'Agostino, P. Favia, F. Fracassi, F. Palumbo, in *16th International Symposium on Plasma Chemistry (ISPC), Taormina, Italy, 2003*, p. 22
142. V. Kovalev, N. Afonina, V. Gromov, Effect of physical adsorption on heat fluxes to catalytic surfaces in carbon dioxide, in *Rarefied Gas Dynamics, 23rd International Symposium*, edited by A.D. Ketsdever, E.P. Muntz, AIP Conference Proceedings (American Institute of Physics, Melville, New York, 2002), pp. 1001–1007
143. F. Zaera, C.S. Gopinath, J. Chem. Phys. **116**, 1128 (2002)
144. V. Guerra, J. Loureiro, Plasma Sources Sci. Technol. **13**, 85 (2004)
145. V.Lj. Marković, Z.Lj. Petrović, M.M. Pejović, Jpn J. Appl. Phys. **34**, 2466 (1995)
146. M.M. Pejović, G.S. Ristić, Č.S. Milosavljević, M.M. Pejović, J. Phys. D: Appl. Phys. **35**, 2536 (2002)
147. M.M. Pejović, E.N. Živanović, M.M. Pejović. J. Phys. D: Appl. Phys. **37**, 200 (2002)
148. R. Engeln, S. Mazouffre, P. Vankan, I. Bakker, D.C. Schram, Plasma Sources Sci. Technol. **11**, A100 (2002)
149. G. Due Billing, *Dynamics of Molecule Surface Interactions* (John Wiley & Sons, Inc., 2000)
150. M. Rutigliano, M. Cacciatore, G.D. Billing, Chem. Phys. Lett. **340**, 13 (2001)
151. N. Sadeghi, C. Foissac, P. Supiot, J. Phys. D: Appl. Phys. **34**, 1779 (2001)
152. D. Blois, P. Supiot, M. Barj, A. Chapput, C. Foissac, O. Dessaux, P. Goudmand, J. Phys. D: Appl. Phys. **31**, 2521 (1998)
153. S. Mazouffre, R. Engelm, P. Vankan, D. Schram, C. Foissac, P. Supiot, N. Sadeghi, Plasma Sources Sci. Technol. **10**, 168 (2001)
154. J.G.E. Beale, H.P. Broida, J. Chem. Phys. **31**, 1030 (1959)
155. P. Supiot, O. Dessaux, P. Goudmand, J. Phys. D: Appl. Phys. **28**, 1826 (1995)
156. C. Gorse, M. Capitelli, A. Ricard, J. Chem. Phys. **82**, 1900 (1985)
157. V. Guerra, P.A. Sá, J. Loureiro, Phys. Rev. E **63**, 046404–1–13 (2001)

158. R. Winkler, D. Loffhagen, F. Sigeneger, in *Advances in Low Temperature RF Plasmas*, edited by T. Makabe (North-Holland, Elsevier, 2002), pp. 50–71

159. V.Lj. Marković, Z.Lj. Petrović, M.M. Pejović, Plasma Sources Sci. Technol. **6**, 240 (1997)

160. V. Guerra, F.M. Dias, J. Loureiro, P.A. Sá, P. Supiot, C. Dupret, Tsviatko Popov, IEEE Trans. Plasma Sci. **31**, 542 (2003)

161. L.S. Bogdan, S.M. Levitskii, E.V. Martysh, Tech. Phys. **38**, 532 (1993)

162. T. Kimura, K. Ohe, M. Nakamura, J. Phys. Soc. Jpn **67**, 3443 (1998)

163. E.I. Toader, Å. Fredriksen, A. Aanesland, Rev. Sci. Instrum. **74**, 3279 (2003)

164. A.A. Kudryavtsev, A.I. Ledyankin, Phys. Scripta **53**, 597 (1996)

165. G. Dilecce, S.D. Benedictis, Plasma Sources Sci. Technol. **2**, 119 (1993)

166. S.D. Benedictis, G. Dilecce, Chem. Phys. **192**, 149 (1995)

167. G. Cartry, L. Magne, G. Cernogora, J. Phys. D: Appl. Phys. **32**, 1894 (1999)

168. M. Capitelli, M. Dilonardo, Rev. Phys. Appl. **13**, 115 (1978)

169. G.E. Caledonia, R.E. Center, J. Chem. Phys. **55**, 552 (1971)

170. E. Plönjes, P. Palm, J.W. Rich, I.V. Adamovich, W. Urban, Chem. Phys. **279**, 43 (2002)

171. S. Saupe, I. Adamovich, M.J. Grassi, J.W. Rich, R.C. Bergman, Chem. Phys. **174**, 219 (1993)

172. L. Lefèvre, T. Belmonte, H. Michel, J. Appl. Phys. **87**, 7497 (2000)

173. E. Eslami, C. Foissac, A. Campargue, P. Supiot, N. Sadeghi, Vibrational and rotational distributions in $N_2(A\ ^3\Sigma_u^+)$ metastable state in the short-lived afterglow of a flowing nitrogen microwave plasma, in *XVIth Europhysics Conference on Atomic and Molecular Physics of Ionized Gases (ESCAMPIG) – 5th International Conference on Reactive Plasmas (ICRP) Joint Meeting, Grenoble, France, 2002*, European Physical Society, Vol. 1, pp. 57–58

174. S.D. Benedictis, G. Dilecce, M. Simek, J. Chem. Phys. **110**, 2947 (1999)

175. R. Farrenq, C. Rossetti, G. Guelachvili, W. Urban, Chem. Phys. **92**, 389 (1985)

176. H. Dünnwald, E. Siegel, W. Urban, J.W. Rich, G.F. Homicz, M.J. Williams, Chem. Phys. **94**, 195 (1985)

177. G.D. Billing, C. Coletti, A.K. Kurnosov, A.P. Napartovich, J. Phys. B: At. Mol. Phys. **36**, 1175 (2003)

178. R.L. DeLeon, J. William Rich, Chem. Phys. **107**, 283 (1986)

179. E. Eslami, A. Campargue, C. Foissac, P. Supiot, N. Sadeghi, in *Frontiers in Low Temperature Plasma Diagnostics (FLTPD-V), Villaggio Cardigliano, Specchia (Lecce), Italy, 2003*, p. 213